

W +charm production with massive c quarks in PowHel

G. Bevilacqua,^a M.V. Garzelli,^b A. Kardos,^c L. Toth^c

^a*ELKH-DE Particle Physics Research Group,
H-4010 Debrecen, P.O. Box 105, Hungary*

^b*II. Institute for Theoretical Physics, Hamburg University
Luruper Chaussee 149, D-22761 Hamburg, Germany*

^c*Department of Experimental Physics, Institute of Physics,
Faculty of Science and Technology, University of Debrecen,
H-4010 Debrecen, P.O. Box 105, Hungary*

E-mail: giuseppe.bevilacqua@science.unideb.hu,
maria.vittoria.garzelli@desy.de,
kardos.adam@science.unideb.hu, toth.lorant@science.unideb.hu

ABSTRACT: The hadroproduction of a W boson in association with a charm quark at the Large Hadron Collider is at the centre of current investigations due to its potential to probe the strangeness content of the proton. In this paper we present an implementation of the $W + c$ production process in the PowHel event generator matched to the PYTHIA8 parton shower approach, allowing to obtain predictions for differential cross-sections with NLO QCD accuracy matched to the accuracy of the Shower Monte Carlo event generator. Effects of non-diagonal CKM matrix elements, finite charm quark mass and off-shell W decays including spin correlations are taken into account. We investigate the production of a leptonically decaying W boson in association with either a charmed meson ($W^\pm + D^{*\mp}$) or a charmed jet ($W^\pm + j_c$) and compare our predictions with particle-level measurements by the ATLAS and CMS collaborations at $\sqrt{s} = 7$ and 13 TeV. Considering the level of agreement between theory predictions and experimental data in the light of present theoretical and experimental uncertainties, our results do not point to the need of extensive modifications of the strange and antistrange distribution functions in the NLO PDF fits that we used, although collider $W + c$ production data have not been included yet in these fits.

KEYWORDS: QCD, NLO computations, heavy quarks, hadronic colliders, parton distribution functions

Contents

1	Introduction	1
2	Computational setup	5
2.1	Details of the implementation	5
2.2	Input parameters	6
2.3	W off-shellness and spin correlation effects	9
3	Phenomenological results	11
3.1	Comparison with CMS data: $W^\pm + D^*(2010)^\mp$ production at 13 TeV	11
3.2	Comparison with ATLAS data: $W^\pm + D^\mp$ and $W^\pm + j_c$ production at 7 TeV	20
4	Conclusions	25
A	Conversion to the decoupling scheme	29

1 Introduction

Various processes involving the production of heavy flavours at hadron colliders are interesting probes of the internal structure of the proton, expressed in terms of parton distribution functions (PDF) at leading twist in collinear factorization [1]. On the one hand, single inclusive heavy-meson production has been used to constrain gluon and the sea quark PDFs in longitudinal momentum fraction regions not covered by the HERA data [2–4]. On the other hand, the production of a W boson in association with a charm quark either fragmenting into an isolated D -meson reconstructed through its decay products or generating a c -jet j_c (hereafter we denote both possibilities by $W + c$, collectively indicating, with a slight abuse of notation, both the $W^+ + \bar{c}$ and the $W^- + c$ cases), can provide important information on strange-quark PDFs and the sea quark flavour composition, for which large uncertainties still exist [5–7]. In particular, beside deep-inelastic-scattering (DIS) HERA data, legacy datasets included in PDF fits to constrain the strange sea include DIS dimuon data from massive high-density detectors, bubble chamber and nuclear emulsion data on charmed hadron production. The incapability of obtaining good fits of all these datasets simultaneously, has led the PDF collaborations to discard or question the validity of some of them. Recent precise Large Hadron Collider (LHC) data (in particular Drell-Yan production) are also sensitive to strange quark distributions.

Their incorporation in PDF analyses has also disclosed potential tensions with part of the aforementioned legacy datasets. The present understanding of proton strange sea is thus still far from being satisfactory. While waiting for new DIS measurements capable of probing sea quarks at a proposed Large Hadron-Electron Collider [8] or at a forthcoming Forward Physics Facility [9] during the High-Luminosity LHC phase, investigating the information we can extract from the $W + c$ process at the LHC nowadays is indeed timely. In fact this process is sensitive to the strange-quark PDF at leading order (LO) accuracy (see Figure 1). The sensitivity to strange PDF sea is

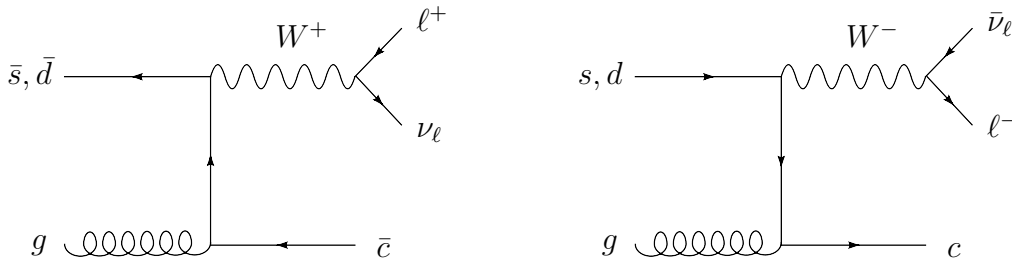


Figure 1. Feynman diagrams describing $W + c$ production at LO accuracy.

somehow weakened by the fact that the Cabibbo-Kobayashi-Maskawa (CKM) matrix is non-diagonal and by the inclusion of radiative corrections, which involve the opening of additional channels at next-to-leading order (NLO) (gg , $q\bar{q}$, qq' , $\bar{q}\bar{q}'$). At the LHC, $W + c$ can probe strange-quark PDFs at scales Q of the order of the W mass. This scale is larger than the typical $Q \sim 1 - 10$ GeV reach of the aforementioned legacy DIS experiments traditionally used to probe the strange-quark distribution. Precise measurements of the cross section ratio $\mathcal{R} = \sigma(W^+ + \bar{c})/\sigma(W^- + c)$ can highlight the degree of asymmetry between s and \bar{s} PDFs and help constraining the strangeness suppression factor $R_s = (s + \bar{s})/(\bar{u} + \bar{d})$. The \mathcal{R} ratio is also sensitive to the V_{cd} parameter of the CKM matrix, whose impact on the $W^- + c$ channel is substantially larger than on $W^+ + \bar{c}$ due to the fact that in pp collisions the d -quark induced parton luminosity is larger than the \bar{d} -quark induced one.

On top of that, $W + c$ is a background for intriguing Standard Model (SM) processes such as $WH(H \rightarrow c\bar{c})$ production, for which experimental analyses have started to be performed only recently [10, 11], and for more known processes, such as single t -quark or $t\bar{t}$ quark production. Beyond the SM, it plays a role in searches of Dark Matter final states accompanied by jets [12–14], and in models with an extended Higgs sector, *e.g.* two-Higgs doublet models [15] with a Higgs boson decaying into a $c\bar{c}$ pair.

Given all these reasons, $W + c$ production has received considerable attention in the last two decades. The first measurements of $W + c$ cross sections have been carried out at the Tevatron by the CDF and D0 experiments [16–18] collected limited data for $W + j_c$, while more recent measurements have been performed at the LHC in Run

I and II by the ATLAS (at 7 TeV) and CMS (both at 7 and 13 TeV ¹) collaborations [20–22] for both $W + D$ meson and $W + c$. Results for $W + c$ production in the forward region are also available by the LHCb collaboration [23].

The high phenomenological interest discussed above motivates this work, where we present, in the same framework, predictions for both $W + D$ -meson and $W + j_c$ production in pp collisions and compare them to the LHC ATLAS and CMS experimental data at the particle level².

Next-to-leading order (NLO) QCD predictions for $W + c$ production in hadronic collisions are available since a while [24] and the complementarity of Drell-Yan and $W + c$ studies to better constrain NLO PDF fits has already been enlightened some time ago [25]. Meanwhile further progress has been achieved with the computation of EW corrections and combined NLO QCD+EW results (see references in Ref. [26]).

Predictions for $W + c$ hadroproduction at NLO QCD accuracy matched to Parton Shower (PS) according to the MC@NLO matching framework can be obtained using the `MadGraph5_aMC@NLO` framework [27], with appropriate modifications of the default version ³. Predictions for $W + c$ hadroproduction according to the POWHEG NLO+PS matching framework [28, 29] with W bosons decaying leptonically are presented here for the first time, by making use of the `PowHel` event generator, including charm-quark mass in the hard-scattering matrix-elements, treating the W off-shell, as well as including non-diagonal CKM matrix effects. `PowHel` produces events at the first radiation emission level in the Les Houches Event Format (LHEF). Further radiation emissions are simulated by an interface to standard Shower Monte Carlo (SMC) codes.

Very recently, the first, state-of-the-art predictions for $W + j_c$ production at NNLO accuracy were presented in Ref. [26], working in a five flavour number scheme, therefore neglecting charm quark mass effects. In an effort to complement this ground-breaking calculation, in this work we show predictions for $W + D$ -meson production retaining charm quark mass effects in the hard-scattering matrix-elements, evaluated in the decoupling renormalization and factorization scheme [30] with three active flavours. We also show predictions for $W + j_c$.

A direct comparison of the predictions in the work of Ref. [26] with the experimental data on differential cross-sections at the particle level is not possible. This is due, on the one hand, to the lack of parton shower and hadronization effects in jet formation (a c -jet for the $W + c$ process at NNLO with five active flavours is formed by one massless charm quark and at most two additional massless partons), whereas

¹A further analysis at $\sqrt{s} = 8$ TeV has been presented in a CMS note [19], but the corresponding paper has not been completed yet.

²In our paper we use particle level for hadron level to be in accord with terminology used by the experiments.

³To activate the possibility of massive charm quarks in the `MadGraph5_aMC@NLO` hard-scattering matrix-elements one has to activate a customized input model file.

an experimental jet is obtained by clustering many hadrons, instead of a few partons. The experimental collaborations, in some analyses, in order to facilitate comparisons with fixed higher-order predictions unfold their fiducial results from the particle to parton level, but this procedure introduces additional systematic uncertainties, depending on the underlying assumptions. On the other hand, the jet algorithm used in the experimental analyses so far (anti- k_T [31]) is not applicable to heavy-flavour jet studies at NNLO. This implied that the authors of Ref. [26] had to use a different algorithm (flavoured- k_T algorithm [32]). On a complementary side in the case of a NLO+PS computation, like the one that we present in this work, the accuracy of the hard-scattering matrix-elements is lower (NLO instead of NNLO on inclusive predictions), however parton shower, hadronization, multiple parton interaction and beam remnant effects are included, allowing for a more realistic modeling of hadronic observables. We use the anti- k_T jet algorithm like in the already available LHC experimental analyses. Let us note that, at NLO accuracy, the use of the anti- k_T jet algorithm is still legitimate for heavy-flavour jets.

The main focus of our study is $W + D$ -meson production, which allows for looser experimental p_T cuts compared to the case of $W + j_c$. For the production of identified hadrons, the complications related to the jet algorithm choice are not present. However, uncertainties exist on the hadronization process. Uncertainties regarding the heavy-quark treatment in parton shower evolution are present for both the j_c and D -meson case.

We also observe that the experimental collaborations so far have employed $W + \text{jets}$ samples of simulated events with hard-scattering matrix-elements evaluated considering five active flavours for their published analyses of the $W + c$ data at particle level. On the other hand, they have used predictions with massive charm as available in various NLO integrators for comparison with their data unfolded to the parton level.

After various studies of the compatibility of strange quark distributions traditionally extracted from legacy DIS data sets with the LHC $W + c$ data (see e.g. Ref. [5]), the PDF collaborations have already started to include the LHC $W + c$ production data in their fits. In particular, we expect that the $W + c$ data analyzed in this paper will also be included in the forthcoming release of the NNPDF PDF fit, i.e. NNPDF4.0 [33], after the recent study of Ref. [7] using as a basis the NNPDF3.1 PDF fit [34], which has lead to various variants of the latter, identified by the prefix **str** (for strange quark). Some of these variants include the LHC $W + c$ production data compared with fixed-order NLO predictions supplemented by a NNLO K -factor although, in the absence of NNLO predictions for the $W + c$ case with massive charm, the calculation of a NNLO K -factor is indeed challenging. Additionally, such a comparison is possible only for experimental data unfolded at the parton level. A part of these data (i.e. those in Ref. [20]) has also been included in the very recent MSHT20 PDF fit [35]. The CT18 collaboration, although not including the LHC $W + c$ data

in their fit [36], has benchmarked their NNLO PDF fits with respect to the ATLAS $W + j_c$ data [21], without, however, using them in association with a full NNLO calculation of partonic cross-sections. We expect that our work provides new insights about including the LHC $W + c$ data in PDF fits and a new method for getting predictions at NLO + SMC accuracy.

The paper is organized as follows. In Section 2.1 we present the computational framework that we used for this work and discuss the setup of the calculation, as well as the various options for modelling W production and decay available in our $W + c$ implementation. In Section 3 we discuss phenomenological results for differential cross sections adopting the cuts used by the LHC experimental analyses. Finally in Section 4 we draw our conclusions.

2 Computational setup

2.1 Details of the implementation

This work is based on the `PowHel1` event generator, built on the interface between the `POWHEGBOX-v2` computing framework [37], which implements the POWHEG NLO+PS matching [28, 29], and `HELAC-NLO` [38], which provides all matrix elements. Infrared divergences are regularized by using the Frixione-Kunszt-Signer subtraction scheme [39, 40], as implemented in the `POWHEGBOX-v2`. The subtraction of the residual initial-state collinear divergences is achieved in the decoupling factorization scheme. The output of `PowHel1` are events at the first radiation emission level, i.e. after the emission of the first additional resolved or unresolved radiative parton. These are collected in files with Les Houches event format (LHEF). Further radiative emissions, as well as the hadronization and hadron decays, can be described by providing these files as an input to SMC programs, including various versions of `PYTHIA` [41–43] and `HERWIG` [44–46]. This way, fully exclusive differential cross-sections for many different observables at the hadron level can be computed.

The `PowHel1` event generator was originally developed for phenomenological studies of top-antitop hadroproduction in association with a range of different particles. In particular, predictions have been presented for several top-quark pair related processes at both the Tevatron and the LHC, and used by the experimental collaborations in a variety of SM and BSM analyses. LHEF events for all these processes were generated in the $\overline{\text{MS}}$ renormalization and factorization scheme with 5 active flavours at all scales above the bottom threshold. The `PowHel1` extension to the decoupling scheme with 4 active flavours at all scales was discussed in Ref. [47], where predictions for $t\bar{t}b\bar{b}$ hadroproduction with massive bottom quarks were compared to those with massless bottom previously obtained [48].

In this paper, for the first time, we have extended `PowHel1` to the decoupling scheme with 3 active flavours, which has required the extension of `HELAC-1LOOP`, part

of `HELAC-NLO`, to include mass effects of c -quarks in all aspects of the computation. Consistently, PDFs in the decoupling scheme with 3 active flavours together with their associated α_S evolution have been used as input of the hard-scattering process. Several PDF sets extracted according to this scheme are available in the LHAPDF interface [49]. However, only part of them include a number of eigenvectors, allowing for an estimate of PDF related uncertainties. The ABMP16.3_NLO PDF fit, that we choose as default in this study, is one of such cases.

In our analysis we also used examples of PDF sets and corresponding α_S in the $\overline{\text{MS}}$ scheme. To be able to use these with hard-scattering matrix-elements with a massive charm quark, in general, a compensation term is needed [50] which appropriately modifies both the coupling and structure functions to decouple the massive degree of freedom⁴. This compensation term is process dependent and the derivation suitable for our purposes can be found in Appendix A.

The `HELAC-NLO` matrix elements have been extensively checked against the public code `MadGraph5_aMC@NLO`. We have also performed comparisons at the integrated level, checking our NLO fixed-order predictions against the public code `MCFM` [51], under different systems of cuts. In all cases we found perfect agreement.

New updates and features have been also implemented in the `PowHel` framework. These include an interface to the `POWHEG-BOX-V2` and the implementation of a general-purpose phase space generator that can be used for generic multi-leg processes. In the all-purpose multi-channel phase space generator we take into account both s - and t -channel branchings. For intermediate massive particles with finite width our phase-space generator maps away the Breit-Wigner resonances. The phase space is constructed using channels. The possible channels are determined by examining the contributing subprocesses undoing particle branchings in all possible ways.

The new `PowHel` version used in this paper got equipped with machinery to fully automatically determine all non-zero helicity configurations for each of the subprocesses. It only uses a minimal set of subprocesses to obtain all the others by means of crossing.

2.2 Input parameters

We consider the processes $pp \rightarrow \ell^+ \nu_\ell \bar{c} + X$ and $pp \rightarrow \ell^- \bar{\nu}_\ell c + X$ at NLO QCD accuracy, *i.e.* the hard scattering is computed at $\mathcal{O}(\alpha_s^2 \alpha^2)$. Here and in the following we denote with ℓ either an electron, a muon or a tau lepton, all considered massless in the computation of the matrix elements. For this reason the latter are only implemented for the electron channel and reused for the other lepton generations. The possible decay channels can be set through the `PowHel vdecaymode` reserved

⁴In the currently available $\overline{\text{MS}}$ PDF sets and corresponding α_S evolution, the number of active flavours below each threshold decreases by just one unity, *i.e.* it switches from 5 light flavours to 4 and 3 light flavours below the bottom and charm thresholds, respectively.

word in the input card ⁵, used for several W boson related processes in POWHEGBOX-v2. For brevity, in the following we will also refer to the above-mentioned processes as to $W^+\bar{c}$ and W^-c . However it should be clear that we consider realistic final states with hadrons, charged leptons and missing transverse momentum. Also, unless stated explicitly, no on-shell approximation is applied to model W boson decays.

The CKM matrix is assumed to be non-diagonal. More precisely we consider the approximation where mixing occurs only between the first two generations of quarks, using $\sin^2\theta_{\text{Cabibbo}}^2 = 0.050934360$ as mixing parameter. Based on this choice, the list of partonic subprocesses that contribute to $W^+\bar{c}$ and W^-c production can be obtained via crossing from the following master amplitudes:

$$\begin{aligned} \emptyset &\rightarrow \ell^+ \nu_\ell \bar{c} s g & \emptyset &\rightarrow \ell^- \bar{\nu}_\ell c \bar{s} g \\ \emptyset &\rightarrow \ell^+ \nu_\ell \bar{c} d g & \emptyset &\rightarrow \ell^- \bar{\nu}_\ell c \bar{d} g \end{aligned} \quad (2.1)$$

$$\begin{aligned} \emptyset &\rightarrow \ell^+ \nu_\ell \bar{c} s gg & \emptyset &\rightarrow \ell^- \bar{\nu}_\ell c \bar{s} gg \\ \emptyset &\rightarrow \ell^+ \nu_\ell \bar{c} d gg & \emptyset &\rightarrow \ell^- \bar{\nu}_\ell c \bar{d} gg \\ \emptyset &\rightarrow \ell^+ \nu_\ell \bar{c} s q \bar{q} & \emptyset &\rightarrow \ell^- \bar{\nu}_\ell c \bar{s} q \bar{q} \\ \emptyset &\rightarrow \ell^+ \nu_\ell \bar{c} d q \bar{q} & \emptyset &\rightarrow \ell^- \bar{\nu}_\ell c \bar{d} q \bar{q} \\ \emptyset &\rightarrow \ell^+ \nu_\ell \bar{c} \bar{u} d & \emptyset &\rightarrow \ell^- \bar{\nu}_\ell c \bar{c} u \bar{d} \\ \emptyset &\rightarrow \ell^+ \nu_\ell \bar{c} \bar{u} s & \emptyset &\rightarrow \ell^- \bar{\nu}_\ell c \bar{c} u \bar{s} \end{aligned} \quad (2.2)$$

where $q \in \{u, d, s\}$. The subprocesses in Eq. (2.1) contribute to the virtual part of the NLO cross section as well as to the integrated subtraction terms, while the ones in Eq.(2.2) contribute to the real part. Other input parameters used in our computation are:

$$\begin{aligned} G_F &= 1.16639 \cdot 10^{-5} \text{ GeV}^{-2}, & m_t &= 172.5 \text{ GeV}, \\ m_b &= 4.75 \text{ GeV}, & m_c &= 1.5 \text{ GeV}, \\ m_W &= 80.379 \text{ GeV}, & \Gamma_W &= 2.085 \text{ GeV}. \end{aligned} \quad (2.3)$$

We work in the G_μ scheme and the electromagnetic coupling α is derived according to the formula

$$\alpha = \frac{\sqrt{2}}{\pi} G_F m_W^2 \sin^2 \theta_W, \quad (2.4)$$

where $\sin^2 \theta_W = 1 - m_W^2/m_Z^2$. Leptonic mass effects are neglected in the calculation of the matrix elements. However for compatibility with PYTHIA8, for which the default values of all lepton masses are non-zero, we restore leptonic masses at the

⁵If n_ℓ corresponds to the lepton family $\ell = e, \mu, \tau$, the ensemble of the allowed decay channels can be set through `vdecaymode = 100 · ne + 10 · nμ + nτ`. Using $n_\ell = 1(0)$ for each channel, the channel is turned on (off).

stage of generation of `PowHel` events. This is done by rescaling momenta such that energy and momentum conservation as well as masses of resonances are preserved⁶. For the leptonic masses we use the same values encoded in the SMC generator: $m_e = 0.511 \cdot 10^{-3}$ GeV, $m_\mu = 0.10566$ GeV, $m_\tau = 1.77699$ GeV.

In this study we will present results obtained with the following PDF sets: ABMP16_3_NLO [52], CT18NLO [53] and CT18ZNLO [53], emerged from QCD analyses including different experimental data. Additionally, the analyses performed by the ABMP16 and CT18 collaborations are based on different theory input, heavy-flavour and α_S treatment, different PDF parameterizations and different treatment of uncertainties and tolerance criterion. A more comprehensive study of PDF uncertainties, which implies the use of all possible NLO PDF fits with all respective eigenvectors available for each PDF set [1] is indeed possible within our framework, but is beyond the scope of this work.

Each PDF set is provided by the respective PDF collaboration together with a specific value of the strong coupling α_S at the M_Z scale. The two-loop running of α_S , consistent with NLO calculations, is provided by the LHAPDF interface. Let us note that the ABMP16_3_NLO PDF set has three active flavours at all scales. The ABMP16 PDF family was derived in a QCD analysis adopting the decoupling scheme for computing the theory predictions used, together with a selection of experimental data, as input to the fit. On the other hand, the CT18 and CT18Z PDF families were derived using a Variable Flavour Number Scheme approach. The CT18 analysis is regarded as one of the global PDF fits. In case of CT18NLO and CT18ZNLO PDFs, a three-flavour version is not yet available⁷. In order to use the latter sets in our computations, the matrix elements that `HELAC-NLO` provides in the decoupling scheme have to be properly modified by compensating terms, as already mentioned in section 2.1. The explicit calculation (see Appendix A) shows that the compensating terms are identically zero when the factorization scale, governing the factorization and PDF evolution, and the renormalization scale, governing α_S evolution, are assumed to be equal.

As for any fixed-order calculation, the hard process contains a residual dependence on the renormalization and factorization scales (denoted by μ_R and μ_F respectively). We consider $\mu_R = \mu_F = \mu_0 = H_T/2$ to be our default scale choice, where

$$H_T = \sqrt{p_{T,W}^2 + m_W^2} + \sqrt{p_{T,c}^2 + m_c^2}. \quad (2.5)$$

Here $p_{T,W}$ is the transverse momentum of the W boson reconstructed from its decay products. This scale is evaluated using the kinematics of the underlying Born process. Uncertainties stemming from variation of scales are estimated by rescaling $\mu_R = \xi_R \mu_0$

⁶This is done by the built-in `lhefinitemasses` routine of `POWHEGBOX-v2`.

⁷The CT18 collaboration is currently working on such a PDF fit version [54].

and $\mu_F = \xi_F \mu_0$, using the standard seven combinations

$$(\xi_R, \xi_F) = \{(0.5, 0.5), (0.5, 1), (1, 0.5), (1, 1), (1, 2), (2, 1), (2, 2)\} . \quad (2.6)$$

The scale uncertainty band is defined taking the upper and lower bounds of the envelope of predictions obtained with these scale choices.

By default in the POWHEG matching the Sudakov peak is produced by exponentiating the whole real-emission contribution. All-order effects should only affect the low- p_T region of extra parton emission. However, as it was shown in [55], there can be processes where this method results in an increase of yield in the high p_T region as well. As a remedy to this problem the `hdamp` option was introduced [55] in order to only exponentiate a part of the real-emission. With a careful selection of the damping function it was achievable to reproduce the fixed-order curve at high- p_T , while simultaneously having a Sudakov shape at low- p_T .

For the Sudakov peak formation the real-emission contribution is used in the form of ratio of the real-emission and Born squared matrix elements. There can be processes where the Born squared matrix element vanishes at phase space points. This results in a numerical instability and was circumvented by the introduction of the `flg_bornzerodamp` parameter which excludes the real-emission contribution from the exponentiation if it is at least five times larger than the subtractions [56]. For the process at hand the Born contribution is finite in all phase-space points, because the charm quark mass is finite, although having a small value when compared with some of the other characteristic scales of the process. The `bornzerodamp` parameter can also be used to improve the efficiency of event generation by excluding those phase-space regions where the extra parton emission is well-resolved, but because of a peaking contribution could negatively affect the event generation, considering the hit-and-miss technique applied at this purpose. The Sudakov peak is the consequence of the all-order summation of Sudakov logarithms. Since Sudakov logarithms have an infra-red origin, the regions where these logarithms are not dominating should not have an effect in the formation of the Sudakov peak.

Extensive studies were carried out and it was found that, beside setting the flag `flg_bornzerodamp` to one, no special damping factor is needed to reach a good efficiency in event generation for the process at hand, have the desired Sudakov shape at low- p_T and match the event-level curve to the fixed-order one at large p_T .

2.3 W off-shellness and spin correlation effects

Due to the high efficiency and integrated luminosity reached in the LHC Runs so far, enough statistics was collected to apply sophisticated sets of cuts on events potentially contributing to $W + c$ production. Due to the decaying W and the exclusiveness of cuts it is not at all trivial to establish a priori up to which extent spin correlations are important to make sane predictions. In order to investigate the

effect of spin correlations or the lack thereof, we consider approaches for the modeling of W boson decays:

1. *Full calculation*: in this case the program uses matrix elements where the leptonic final states are present and a finite width is assigned to the W boson. So this option includes full spin correlations in the W decay products with finite width effects for the W .
2. *Narrow width approximation* (NWA): the same matrix elements are being used as for case 1 but the Breit-Wigner resonance of the W is replaced by a Dirac-delta function corresponding to the $\Gamma_W \rightarrow 0$ limit:

$$\left| \frac{i}{p_W^2 - m_W^2 + im_W \Gamma_W} \right|^2 \rightarrow \frac{\pi}{m_W \Gamma_W} \delta(p_W^2 - m_W^2). \quad (2.7)$$

In this approach spin correlations are preserved while finite-width effects of the W boson decay are dropped.

3. *No spin correlation*: a stable W boson is considered in the matrix elements. The on-shell W boson is decayed in the event generation step, prior to the shower evolution, using isotropic decay. This way the SMC receives events with leptonic final state but lacking spin correlations in the decay products.
4. *SMC-decay*: The same matrix elements as for case 3 are adopted. In this approach the W decay is performed directly by the SMC program, which by default does not account for spin correlation effects.

Unless stated explicitly, all predictions shown in Section 3 are based on the *Full Calculation* approach. In Section 3.2 we will also present a comparison of differential NLO+PS cross sections based on the four approaches described above, considering the set of cuts adopted by the ATLAS collaboration in the analysis of $W + c$ at $\sqrt{s} = 7$ TeV. For illustrative purposes, we present here a comparison of fully inclusive predictions for $W^+ + \bar{c}$ production at 7 TeV. These results are obtained from the LHE generated by PowHel and thus refer to the parton level as it emerges after the POWHEG matching. The contribution of $W + c\bar{c}$ final states, part of NLO real radiation, is not included at this stage. The contribution of the $W + c\bar{c}$ final state to the total cross section is at around 5%. Figure 2 shows distributions of the transverse momentum of the charged lepton arising from the W boson decay ($p_{\perp,\ell}$) as well as of the total missing momentum (\cancel{p}_{\perp}). The two plots report the predictions that we obtained using the four above-mentioned approaches, considering the scale setup $\mu = \mu_R = \mu_F = H_T/2$ and the ABMP16_3_NLO PDF set as benchmarks. We observe that predictions labeled with "no spin" and "SMC-decay" are very close to each other. This should not come as a surprise since the two results adopt identical accuracy for

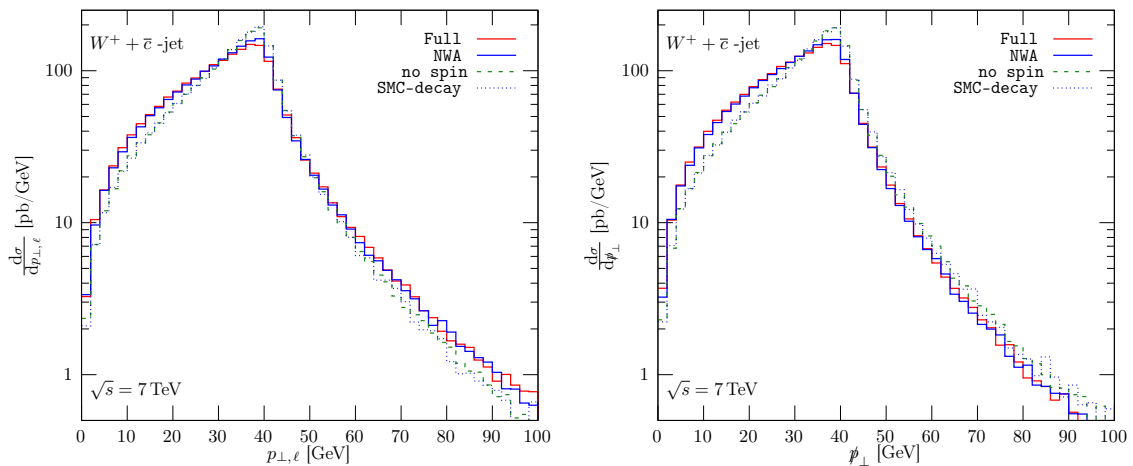


Figure 2. Fully inclusive $W^+ + \bar{c}$ differential cross sections as a function of the transverse momentum of the charged lepton (left plot) as well as of the missing p_T (right plot). Effects from parton shower and hadronization are not taken into account. Results are based on the ABMP16.3_NLO PDF set and on the scale choice is $\mu = \mu_R = \mu_F = H_T/2$.

the modeling of the W boson decay. On the other hand spin correlations (“NWA”) have a visible effect on the shape of both distributions, where low- p_T regions are enhanced for the charged lepton as well as for the missing p_T . It is easily understood that such effect has an impact on the full chain of the calculation up to the level of a realistic NLO+PS predictions, given that the typical setup of the experimental analyses includes minimum requirements on the lepton p_T . For comparison, looking at the prediction labeled with “Full”, one can observe that effects related to the off-shellness of W boson decays play a minor role in this context.

3 Phenomenological results

As mentioned in the Introduction, public results for $W + c$ production at the LHC have been released by both the ATLAS and CMS collaborations. We start the analysis by comparing our theory predictions for D -meson production in association with a W boson decaying leptonically with the data of the CMS analysis at $\sqrt{s} = 13$ TeV [22] and of the ATLAS one at $\sqrt{s} = 7$ TeV [21]. In Ref. [21] ATLAS has also published data on c -jets. We also report a comparison with the latter.

3.1 Comparison with CMS data: $W^\pm + D^*(2010)^\mp$ production at 13 TeV

The CMS analysis of $W^\pm + D^*(2010)^\mp$ events published in Ref. [22] provides differential distributions of the absolute value of the pseudorapidity for the charged lepton associated with the W boson leptonic decay. In particular, a W boson is identified when it decays into a muon ($p_{T,\mu} > 26$ GeV and $|\eta_\mu| < 2.4$) accompanied

by missing energy. Predictions are presented for the individual $W^- + D^*(2010)^+$ and $W^+ + D^*(2010)^-$ channels as well as for their sum.

The potential contribution of the $W^\pm c\bar{c}$ process is greatly suppressed with respect to that of the $W^+\bar{c}$ and W^-c processes through analysis cuts, which make $W^\pm c\bar{c}$ contributing in equal proportion on average to both the signal and the background. In particular, the cross-section contribution of the events where a $D^*(2010)$ -meson is detected with the same charge sign of the hardest central muon identified as coming from W boson decay (background) is subtracted from the one of the events where the muon and the $D^*(2010)$ -meson charges have opposite sign (signal).

As mentioned in the Introduction, on the one hand, the CMS collaboration compared the data at the particle level with simulations of $W^+ \rightarrow \mu^+ \nu_\mu$ ($W^- \rightarrow \mu^- \bar{\nu}_\mu$) production in association with light jets made with `MadGraph5_aMC@NLO` interfaced to `PYTHIA8`. On the other hand, they also unfold their experimental distributions at the parton level, and, in this case, they compare the corresponding results to the fixed-order NLO QCD implementation available in `MCFM`, involving instead massive charm quarks. In their analysis central $D^*(2010)$ -mesons ($|\eta_D^*| < 2.4$) with a relatively low transverse momentum p_{T,D^*} are measured ($p_{T,D^*} > 5$ GeV). This fact motivates the investigation of charm-quark mass effects in the calculation, given that the charm-quark mass ($\sim \mathcal{O}(1 - 2)$ GeV) has the same order of magnitude of the minimum p_{T,D^*} value explored by the experimental collaboration. The p_{T,D^*} distributions are peaked at low p_{T,D^*} values, implying that the typical differential cross-sections for the observables considered in the experimental analysis, which integrate over the whole measured range of p_{T,D^*} , are dominated by the contribution of events with $D^*(2010)$ -mesons with p_{T,D^*} values close to the kinematical cut.

In Fig. 3 we compare the predictions obtained by `PowHel` + `PYTHIA8`, using hard-scattering matrix-elements with massive charm, to the CMS experimental data at the particle level. The three panels report separately differential distributions of the absolute value of the charged muon pseudorapidity for the μ^+ and μ^- cases, as well as their sum. Theory predictions include parton shower, hadronization, multiple particle interaction (MPI) and beam remnant effects, with parameters fixed by the selected `PYTHIA8` tune. We study the effects of two different `PYTHIA8` tunes, by computing theory predictions with both the default Monash tune [57] (option 14 in `PYTHIA8`, current default), used in Fig. 3, and one of the recent ATLAS A14 central tunes [58] (option 21 in `PYTHIA8`), used in Fig. 4. The two selected tune options are both based on the same PDF set (NNPDF2.3 LO [59]) and both incorporate LHC Run I data ($\sqrt{s} = 7$ TeV). On the one hand, the Monash tune was designed with the intent of providing an overall reasonable description of both minimum-bias and underlying event physics, i.e. of both soft-inclusive physics and the processes typically accompanying a hard-scattering (central) collision. On the other hand, the ATLAS A14 set of tunes focused on events with one or more high- p_T emissions, providing a simultaneous tune of both PS and MPI parameters, by making use of ATLAS data

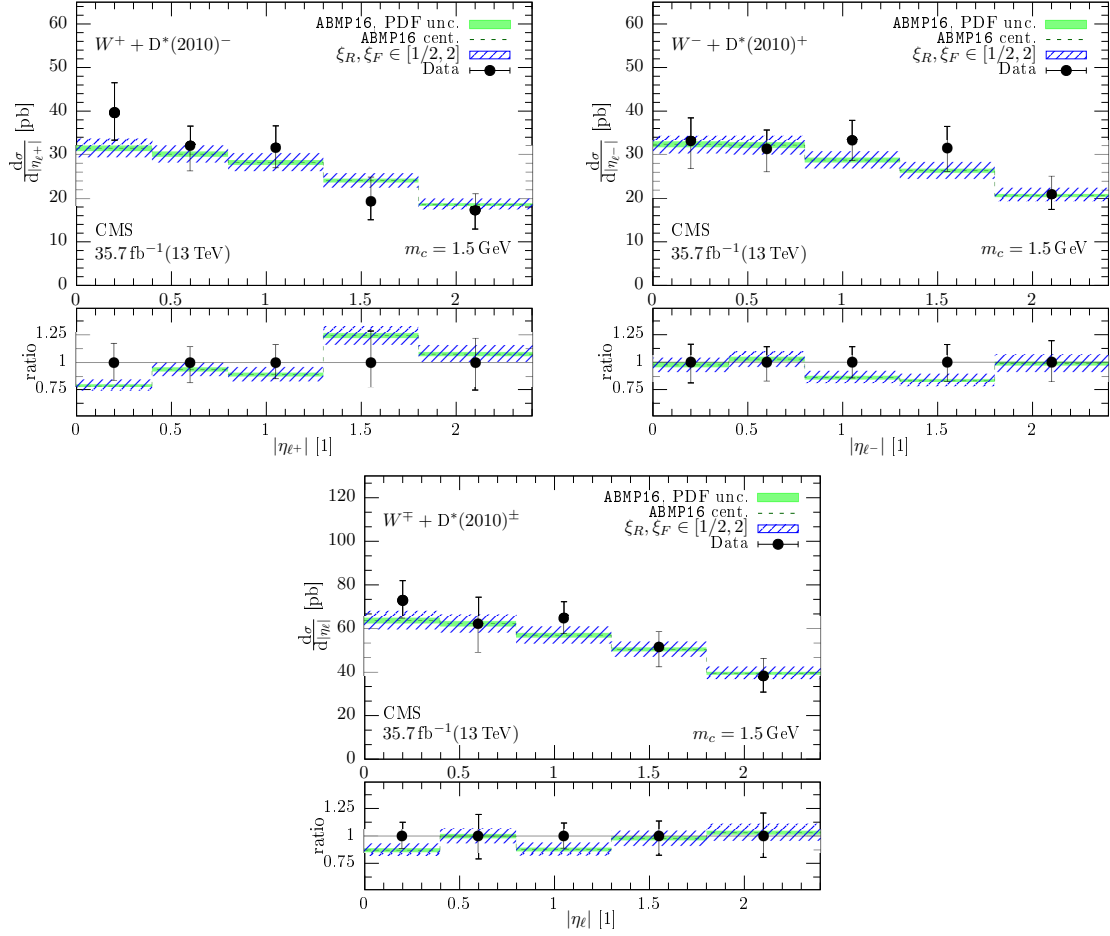


Figure 3. Difference of the differential cross-section for $W + D^*(2010)$ -meson production, with $W^\pm \rightarrow \mu^\mp \nu_\mu^{(-)}$, where the hardest central μ and the $D^*(2010)$ -meson have charge of opposite sign and that where the μ and the $D^*(2010)$ -meson have charges of the same sign, as a function of the absolute value of the pseudorapidity of the hardest μ . The three panels refer respectively to the case of μ^+ , μ^- and their sum. Theoretical predictions at NLO + SMC accuracy, obtained by PowHel1 + PYTHIA8 are compared to experimental data from the CMS collaboration [22]. 7-point (μ_R, μ_F) scale uncertainty and PDF uncertainty bands, computed from the 30 eigenvectors of the ABMP16.3_NLO PDF set, are reported by shaded (blue) and solid (green) bands, respectively. As further input of PowHel1, we consider 2-loop α_S evolution, $\alpha_S(M_Z) = 0.1066$ consistent with the PDF set, and $m_c = 1.5$ GeV. The predictions include parton shower, hadronization, MPI and beam remnant effects according to the PYTHIA8 Monash tune. See text for more detail.

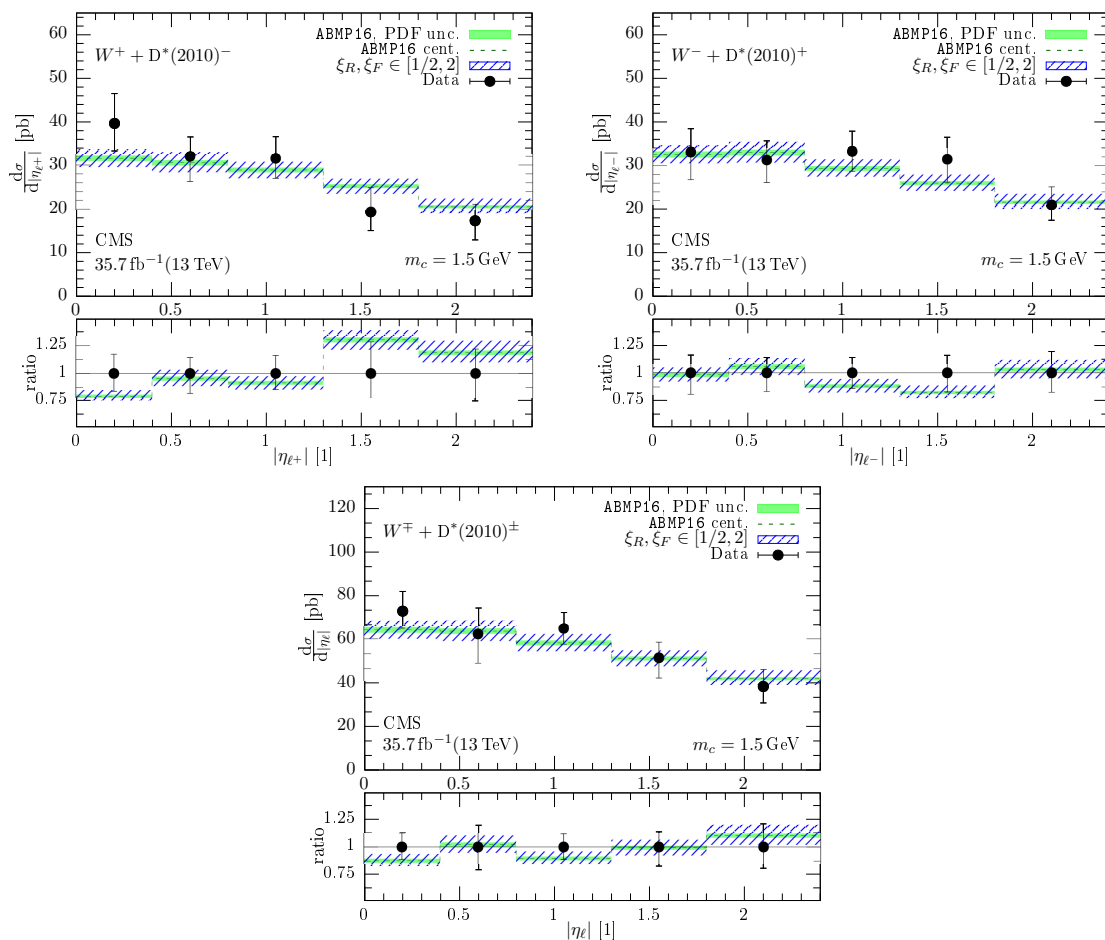


Figure 4. Same as in Fig. 3, but using the PYTHIA8 ATLAS A14 central tune with NNPDF2.3LO PDFs.

for distributions sensitive to initial state interactions, final state interactions and the underlying event. Among others, both tunes included Drell-Yan data. However, the Monash tune, differently from the ATLAS one, also includes CMS data.

While we did not make any attempt to vary the LO PDF corresponding to each tune in the SMC not to spoil the validity of the tune itself, we consider the effect of the variation of the NLO PDF and scales used as input for the generation of the events at the first radiation emission level, by exploiting the reweighting opportunities available within the POWHEGBOX-v2 framework, that we imported in PowHel1. In particular, the hatched (blue) uncertainty bands in Fig. 3 and 4 refer to the 7-point renormalization and factorization scale variation around the central value $(\mu_R, \mu_F) = \mu_0 = H_T/2$, where H_T is computed from the underlying Born according to formula 2.5. The central predictions refer to the AMBP16.3_NLO PDF set, that we use as our default, together with its $\alpha_S(M_Z)^{n_f=3} = 0.1066$ value (cor-

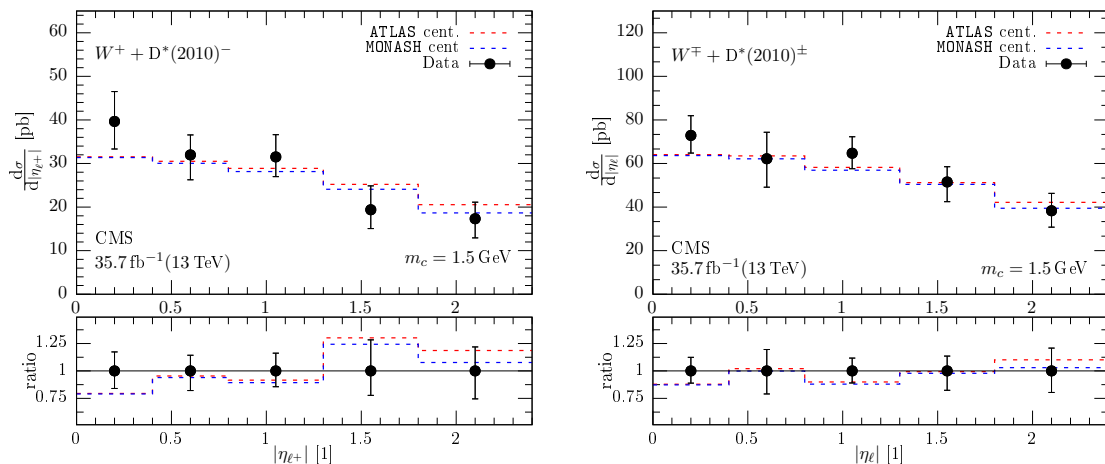


Figure 5. Same as in Fig. 3 and 4, but limited to central predictions with two different PYTHIA8 tunes (Monash and ATLAS A14 central tune with NNPDF2.3LO PDFs). The two panels refer to the μ^+ case (left) and to the $\mu^+ + \mu^-$ case (right), respectively.

responding to $\alpha_S(M_Z)^{n_f=5} = 0.1191$), α_S two-loop evolution and $m_c = 1.5$ GeV⁸. In this case, PDF uncertainties, also shown in Fig. 3 and Fig. 4, amounting to approximately $\pm 2\%$, turn out to be much larger than scale uncertainties, amounting to approximately to $\pm(6 \div 8)\%$ and slightly asymmetric around the central value. Changing tune does not affect in a sizable way the size of the scale and PDF uncertainty bands, that are approximately the same in Fig. 3 and 4. It plays a role, instead, in modifying the normalization and the shape of central predictions, with those obtained with the ATLAS A14 central tune slightly enhanced (up to a factor $\lesssim 10\%$ in the most forward direction) with respect to those with the Monash tune, as shown in Fig. 5.

The conclusion that the PDF uncertainty is smaller than scale uncertainty drawn for the ABMP16_3_NLO PDF case in the discussion of Fig. 3 and 4, does not apply to every PDF set. For example, in case of the CT18NLO and CT18ZNLO PDF sets, PDF uncertainties are larger, as visible in Fig. 6, or of comparable size, as visible in Fig. 7, with respect to scale uncertainties⁹ these modifications are small, i.e. modifi-

⁸The ABMP16 QCD analysis provides a simultaneous fit of PDFs, $\alpha_S(M_Z)$ and heavy-quark mass values, considering the correlations between these quantities. In that framework, the charm mass value is fitted in the $\overline{\text{MS}}$ mass renormalization scheme, obtaining $m_c^{\overline{\text{MS}}} = 1.175 \pm 0.033$ GeV at NLO. The conversion of this value to the pole mass renormalization scheme, that we use in our computation, with coefficients known up to four-loops [60], does not lead to a convergent perturbative expansion in α_S . For more details on conversion formulas between different mass renormalization schemes see e.g. [61].

⁹Scale uncertainty is computed here for the ABMP16_3_NLO PDF fit only. Repeating the computation for the CT18NLO and CT18ZNLO PDF fits, may lead to modifications of the size of the band. However, we expect that for the case study at hand and the considered PDF sets

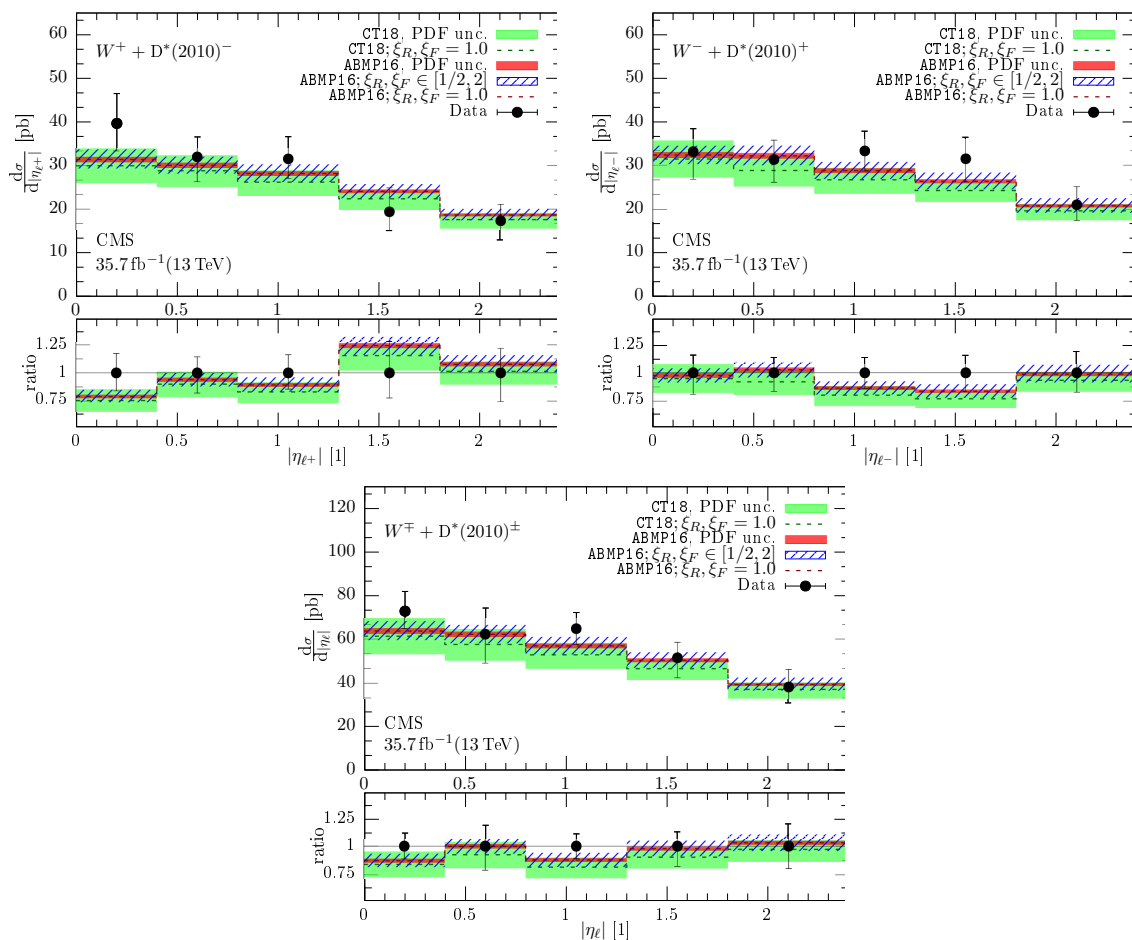


Figure 6. Same as Fig. 3, but using the CT18NLO PDF set, with 2-loop α_S evolution and $\alpha_S(M_Z)^{n_f=5} = 0.118$ consistent with the PDF set, and with $m_c = 1.4$ GeV. Asymmetric PDF uncertainty bands (green solid), computed at 90% C.L. corresponding to the tolerance criterion adopted in this PDF fit, refer to this configuration. Predictions from this configuration are compared to those using the ABMP16_3_NLO PDF set, with 2-loop α_S evolution and $\alpha_S(M_Z)^{n_f=3} = 0.1066$ ($\alpha_S(M_Z)^{n_f=5} = 0.1191$), consistent with the PDF set, and with $m_c = 1.5$ GeV. For the latter, beside PDF uncertainty bands (red solid) computed at 68% C.L. as customary for this PDF fit, we also report scale uncertainties (blue hatched bands).

cations of the percentual size of the scale uncertainty band $\Delta\mu\% \rightarrow \Delta\mu\% \pm (1\div 2)\%$, depending on the tolerance criterion used and, moderately, also by the prescription for computing PDF uncertainties. In particular, the CT18NLO and CT18ZNLO PDF uncertainty bands shown in Fig. 6 and 7 refer to the default prescription provided by the CT collaboration, leading to asymmetric uncertainties at the 90% C.L., corresponding to the tolerance criterion adopted in their QCD analysis and to the fact that, when performing the PDF fit, they did not symmetrize the errorbars

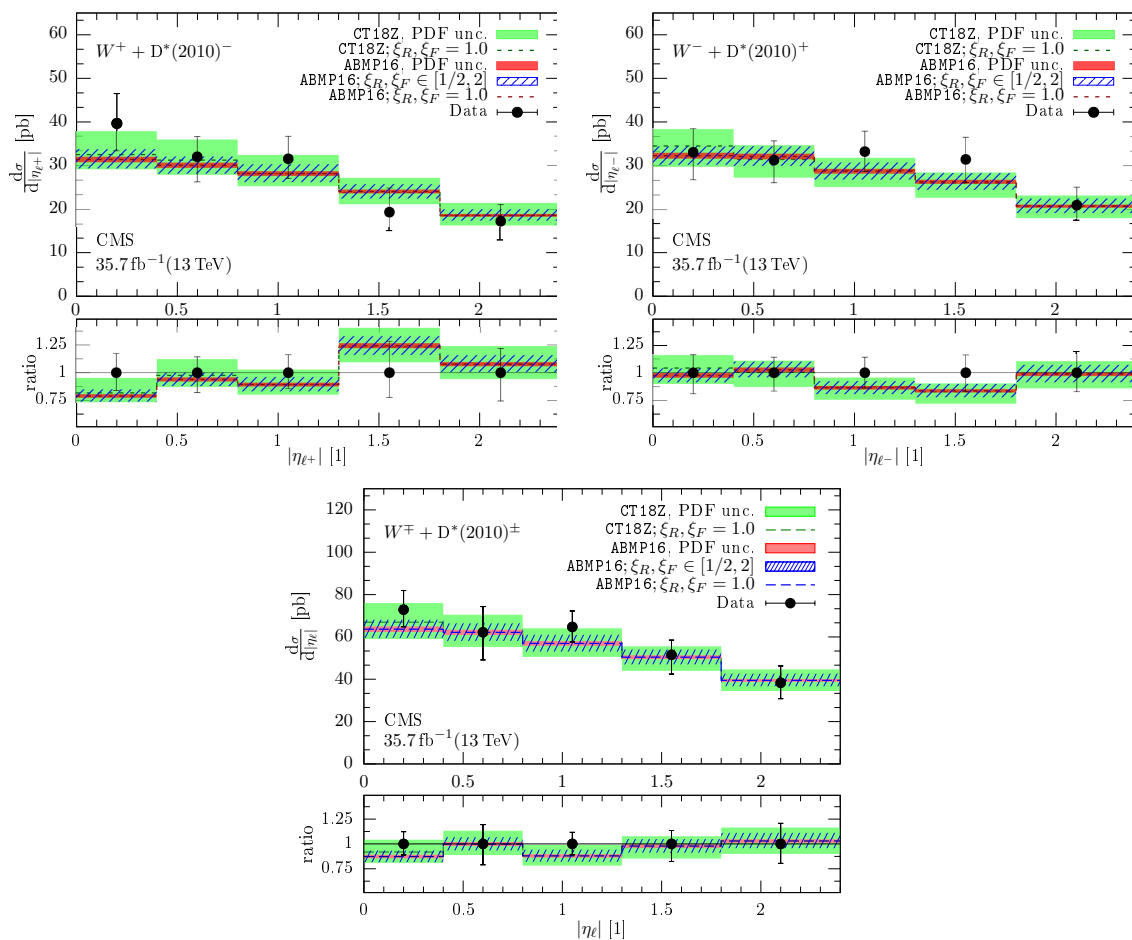


Figure 7. Same as Fig. 6, but using the CT18ZNLO PDF set, with 2-loop α_S evolution, $\alpha_S(M_Z)^{n_f=5} = 0.118$ and $m_c = 1.4$ GeV, consistent with the PDF set. Asymmetric PDF uncertainty bands (green solid), computed at 90% C.L., corresponding to the tolerance criterion adopted in this PDF fit, refer to this configuration. Predictions from this configuration are compared to those using the ABMP16.3_NLO PDF set, with 2-loop α_S evolution and $\alpha_S(M_Z)^{n_f=3} = 0.1066$ ($\alpha_S(M_Z)^{n_f=5} = 0.1191$), consistent with the PDF set, and with $m_c = 1.5$ GeV. For the latter, beside PDF uncertainty bands (red solid) computed at 68% C.L. as customary for this PDF fit, we also report scale uncertainties (blue hatched bands).

of the experimental datapoints included. On the other hand, the CT18NLO and CT18ZNLO PDF uncertainty bands shown in Fig. 8 refer to the symmetrized uncertainty prescription by the CT collaboration. Additionally, in Fig. 8 we have rescaled the CT18NLO and CT18ZNLO PDF uncertainty bands to the 68% C.L. to facilitate the comparison with the ABMP16.3_NLO uncertainty band, which is symmetric by construction, considering that the errorbars affecting the experimental datapoints were symmetrized when performing this PDF fit. This band size corresponds to the tolerance criterion $\Delta\chi^2 = 1$ adopted by default in the ABMP16 PDF fit and

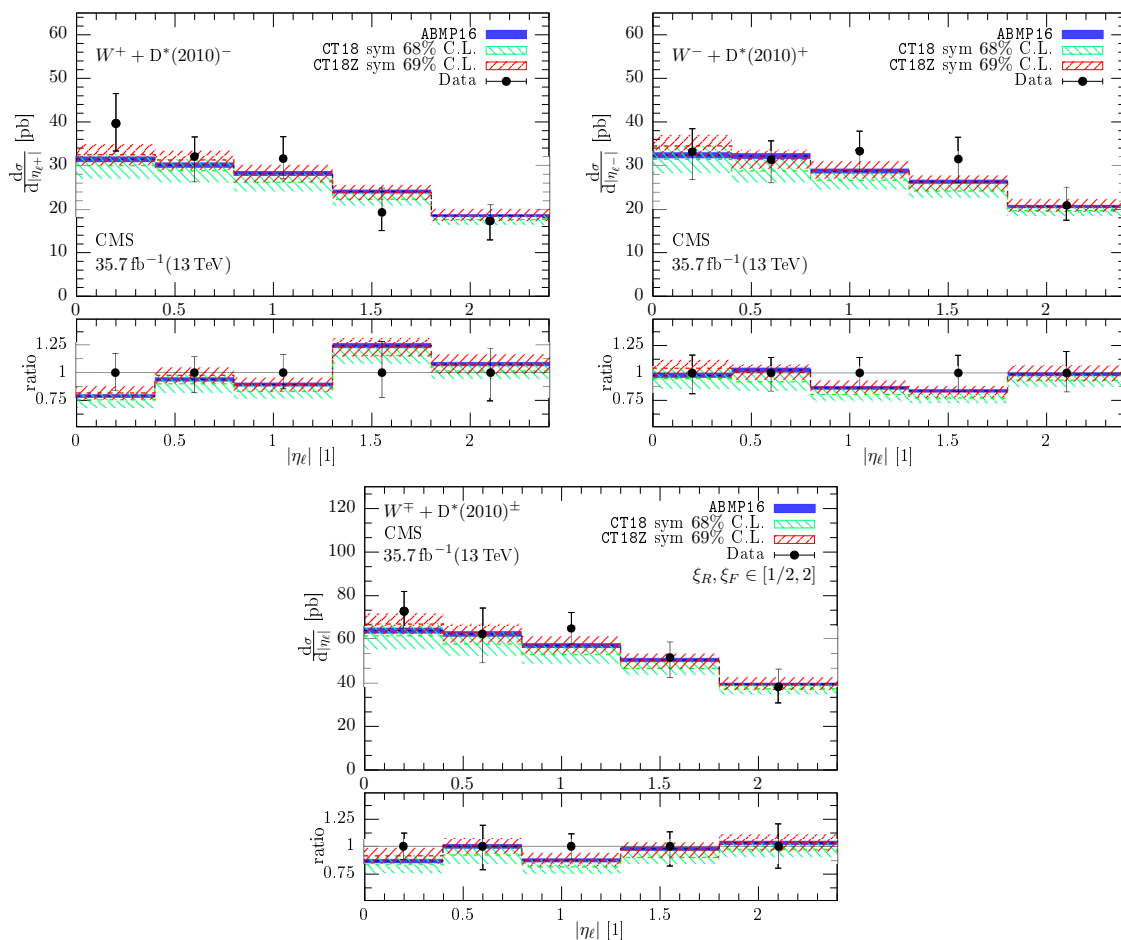


Figure 8. Same as Fig. 3, but using the three different NLO PDF + $\alpha_S(M_Z)$ sets ABMP16_3_NLO, CT18ZNLO and CT18NLO, each one with its own uncertainties. A value of $m_c = 1.5$ GeV is used in association with the ABMP16_3_NLO fit, whereas $m_c = 1.4$ GeV is used in association with the CT18ZNLO and the CT18NLO fits. Differently from Fig. 6 and 7, the CT18NLO and CT18ZNLO uncertainty bands in this figure are symmetrized by computing them with the specific prescription provided by the CT collaboration and scaled to the 68% C.L. to facilitate a more direct comparison with the ABMP16 uncertainty bands, symmetric by fit construction, customarily provided at this C.L. corresponding to the tolerance criterion adopted in the ABMP16 fit.

in many other PDF fits. The residual difference in the size of the PDF uncertainty bands visible in Fig. 8 is related to the different theory and parameterization constraints and data included in the various PDF analyses which have led to these PDF sets. In particular, both the ABMP16 and the CT18ZNLO analyses include recent precise Drell-Yan data at the LHC, which turn out to be quite relevant for constraining flavour separation in quark PDFs¹⁰. These data are instead absent from

¹⁰In PowHe1 we consider PDF fits with NLO accuracy, in full consistency with the perturbative

the CT18NLO PDF analysis. As a consequence, the CT18NLO PDF band is larger ($\sim \pm 10\%$) than the CT18ZNLO ($\sim \pm 8\%$) for central $|\eta_\mu|$. They approach each other in size at the middle of the $|\eta_\mu|$ spectrum, and they end to be roughly of the same size ($\sim \pm 5\%$).

On the other hand, the difference in the absolute value of central predictions when using different PDFs is related partly to the various ingredients of the PDF fit (see discussion above) and partly to the m_c values that we adopted in the computation, i.e. $m_c = 1.4$ GeV for the CT18ZNLO PDF set and $m_c = 1.5$ GeV for the ABMP16.3.NLO PDF set. On the other hand, the CT18NLO PDF fit was performed by the CT collaboration using as input $m_c = 1.3$ GeV, which, for full consistency, we should have also used for predictions with it. Decreasing m_c leads to an increase of the cross-sections. Therefore, if we would have used the latter value, we would have got central predictions slightly enhanced, i.e. in slightly better agreement with the CT18ZNLO and ABMP16.3.NLO PDF cases. We used instead $m_c = 1.4$ GeV to facilitate the comparison with the CT18ZNLO PDF case, considering that the latter were fitted and provided with this m_c value by the CT collaboration.

Overall, when considering their (PDF + scale) uncertainties, our theory predictions with ABMP16.3.NLO and CT18ZNLO PDFs are compatible in all bins with the experimental data. The best theory/data agreement is obtained with the CT18ZNLO predictions. Predictions with the CT18NLO PDFs lie slightly below the previous ones, but, if one considers the nominal uncertainty bands at 90% C.L shown in Fig. 6, the conclusion of agreement with experimental data in all bins apply also to the latter. In all three cases, we observe that the theoretical predictions in the first bin of the μ^+ distribution lie at the lower limit of the experimental data error bars. We believe that the possibility of data migration from the second to the first bin in this distribution has to be better investigated.

On the basis of the size of the NLO+PS scale uncertainty bands, we expect that the inclusion of NNLO corrections in the hard-scattering matrix-elements, will play a moderate effect in modifying the NLO+PS predictions. Notwithstanding the fact that the level of agreement between our theory predictions and the experimental data does not point to an urgent need of important modifications of the PDF sets that we used, we believe that new NLO PDF analyses including $W + c$ data would be valuable, considering the present tensions/inconsistencies among various datasets already included in the PDF analyses, which have made the strange quark one of the

accuracy of the hard-scattering matrix-elements. Recent doubts on the use of Drell-Yan data in NNLO PDF fits have been raised e.g. in Ref. [62], due to the lack of publicly available NNLO integrators for computing fiducial cross-sections for Drell-Yan production capable of accounting for the effects of linear power corrections [63] which can arise in case of symmetric cuts on leptons from W -boson decays. As shown in Ref. [62], the size and presence of these power corrections depends on the adopted NNLO IR regularization method and of the specific analysis cuts, and it is far from being negligible in many experimentally analyzed configurations for various theory setups/tools.

longstanding issues in PDF studies.

Comparing among each other the panels of each of the previously discussed figures, we observe that a better agreement between central theory predictions and experimental data is achieved for the sum of the $W^+ + D^*(2010)^-$ and $W^- + D^*(2010)^+$ production data, than for the data for these two channels considered separately. Considering that W^-c and $W^+\bar{c}$ are sensitive to a different mixture of d and s quarks, including separately both kinds of data in PDF fits is important for quark flavour separation and for strange-antistrange asymmetry studies. In cross-section ratios part of the uncertainties cancel. However, in order to get full advantage from the inclusion of W^-c and $W^+\bar{c}$ absolute cross-section data in the PDF fits, it is crucial that the experimental uncertainties, at the moment much larger than the scale uncertainties from missing higher orders affecting theory predictions and than the PDF uncertainties (at least for some PDF fit), get reduced.

3.2 Comparison with ATLAS data: $W^\pm + D^\mp$ and $W^\pm + j_c$ production at 7 TeV

The ATLAS collaboration published a detailed analysis of $W + c$ production data at $\sqrt{s} = 7$ TeV in Ref. [21], which includes both the $W + D$ -meson and the $W + j_c$ cases, with W decaying leptonically. Similarly to the CMS analysis discussed in the previous section, even in the ATLAS analysis the W bosons are reconstructed from their decay products, and the distribution of the absolute value of the pseudorapidity of the charged lepton ℓ from W boson decay is measured, subtracting the contribution of the events including a D -meson (j_c) with charge having the same sign as the ℓ charge (background) from that of the events where the charge of the D -meson (j_c) and of the ℓ have opposite sign (signal). Like the CMS analysis, the ATLAS analysis reports separately the differential distributions of charged leptons emerging from the decays of W bosons of opposite charge. The ATLAS analysis asks for exactly one isolated lepton in order to reduce backgrounds, and, differently from the CMS analysis, it provides cross-sections for the sum of the muonic and the electronic W boson decay channels, with cuts on the lepton $p_{T,\ell} > 20$ GeV, $|\eta_\ell| < 2.5$, on the missing energy $E_T^{miss} > 25$ GeV, and on the transverse mass of the reconstructed W boson, $m_T^W > 40$ GeV. In the D -meson analysis, the presence of a D -meson is required, with $p_{T,D} > 8$ GeV and $|\eta_D| < 2.2$, whereas in the j_c analysis, the presence of exactly one anti- k_T c -jet ($R = 0.4$) with $p_{T,j} > 25$ GeV and $|\eta_j| < 2.5$, that includes at least a charmed hadron with $p_{T,h_c} > 5$ GeV, is required. The binning considered in the ATLAS D -meson analysis is slightly coarser than the one used in the CMS one (4 bins instead of 5) and covers approximately the same pseudorapidity range. The bin width considered in the ATLAS j_c analysis is much smaller than the one used in case of D -mesons and covers the same pseudorapidity range.

In Fig. 9 we report the comparison of our theory predictions with the $W^\pm + D^\mp$ experimental data. We use the same scale and setup as for the CMS analysis, except

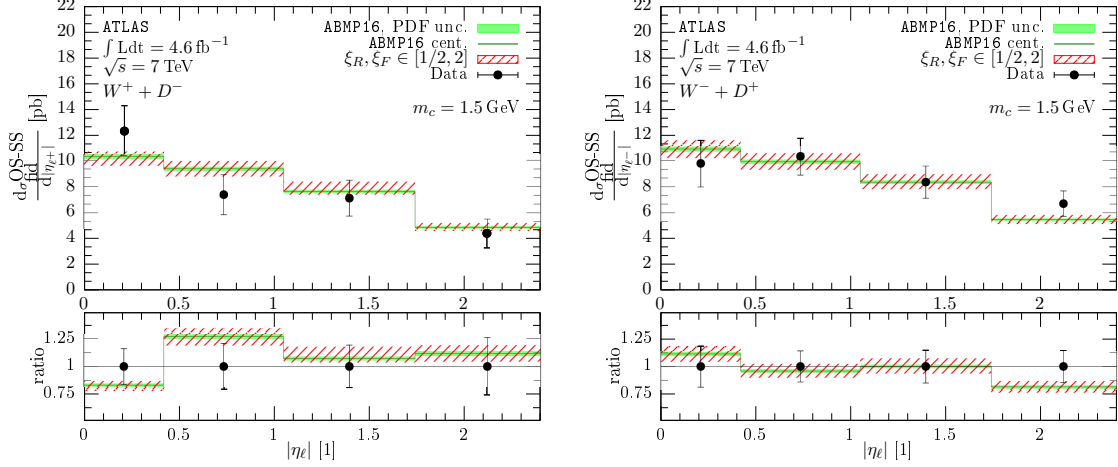


Figure 9. Difference of the differential cross-section for $W + D$ -meson production, with $W^\pm \rightarrow \ell^\pm + \bar{\nu}_\ell$, where the ℓ^\pm and the hardest D^\pm -meson have charges of opposite sign and that where the ℓ^\pm and the D^\pm -meson have charges of same sign, as a function of the absolute value of the pseudorapidity of the lepton. Theoretical predictions at NLO + SMC accuracy, obtained by PowHel1 + PYTHIA8 are compared to experimental data from the ATLAS collaboration [21]. 7-point (μ_R, μ_F) scale uncertainty and PDF uncertainty bands, computed from the 30 eigenvectors of the ABMP16 PDF set, are reported by shaded (red) and solid (green) bands, respectively. The predictions include parton shower, hadronization, MPI and beam remnant effects according to the PYTHIA8 ATLAS A14 central tune with NNPDF2.3LO PDFs.

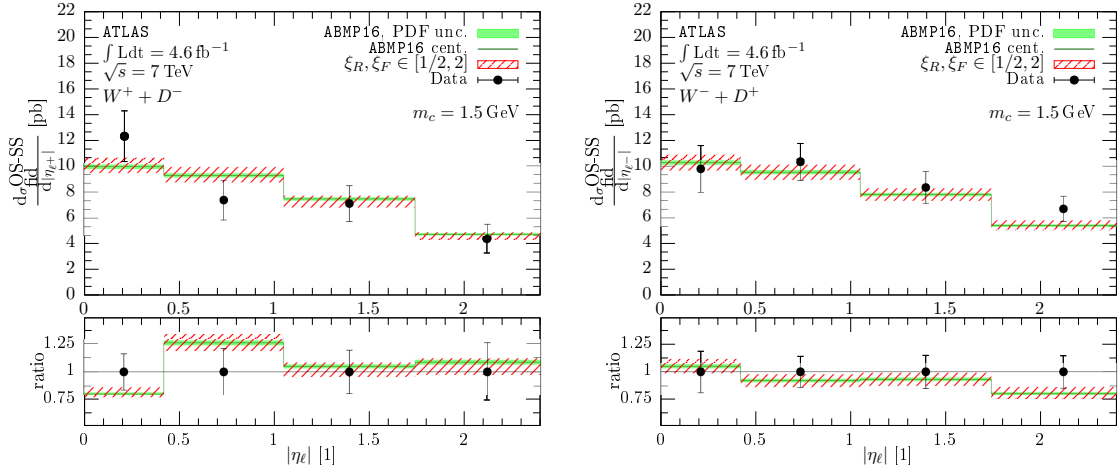


Figure 10. Same as in Fig. 9, but using the PYTHIA8 Monash tune.

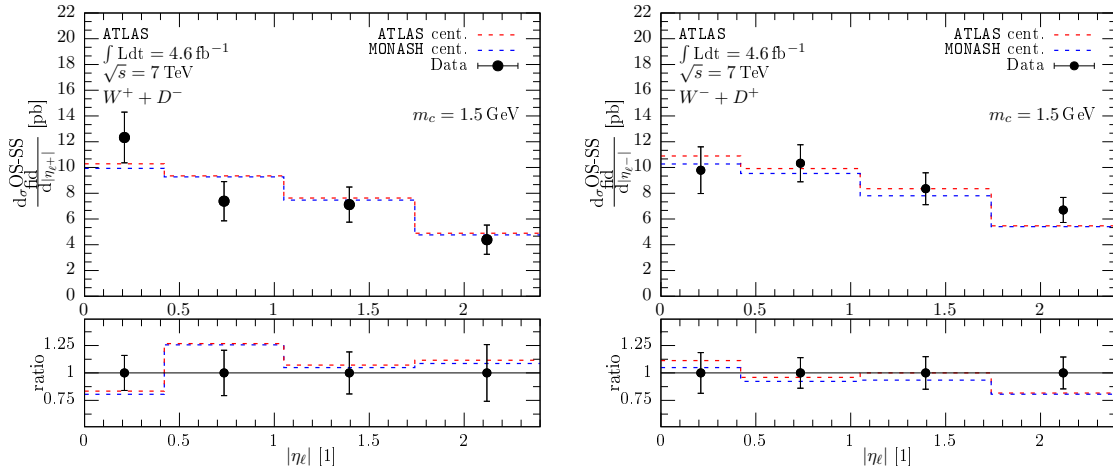


Figure 11. Same as in Fig. 9 and 10, but limited to central predictions with two different PYTHIA8 tunes (Monash and ATLAS A14 central tune with NNPDF2.3LO PDFs).

that, in case of the ATLAS analysis, we use as default the PYTHIA8 ATLAS central A14 tune with NNPDF2.3LO PDFs. The impact of the choice of a different tune is moderate, as can be seen by comparing this figure with Fig. 10 where the Monash tune is instead used. Predictions obtained with both tunes are compared to each other in Fig. 11, from which one can see that they differ by less than 10% (biggest difference being 7%), with the ATLAS A14 tune giving predictions slightly enhanced with respect to the Monash tune in all bins.

We found that the level of agreement between theory predictions and experimental data is similar to the CMS case (see discussion in subsection 3.1). We consider this as a cross-check of the compatibility of the ATLAS and CMS data and a proof of the robustness of our conclusions. In particular, we observe that theory predictions for $(W^\pm + D^\mp)$ production are compatible with ATLAS experimental data, when considering both the theoretical and experimental uncertainties, in almost all bins. The marginal level of agreement of theory predictions with the experimental data in the first two bins of the $|\eta_{\ell^+}|$ distribution might be attributed to bin migration or low statistics effects. In fact the experimental central rapidity datapoint values do not appear to decrease monotonically, as one finds instead for theoretically computed rapidity distributions. Analogous observations applied also to the CMS experimental data, as discussed in Section 3.1. Even the $|\eta_{\ell^-}|$ experimental distribution does not decrease monotonically, differently from our NLO + SMC theory predictions. It reaches a maximum in the second bin. For this distribution, we observe good compatibility of central theory predictions with experimental data in most of the central rapidity bins, as we also noticed in the CMS case.

Scale uncertainties amount to approximately $\pm(6 \div 8)\%$ and are larger than PDF uncertainties, at least when we compute the latter using the ABMP16_3_NLO PDF

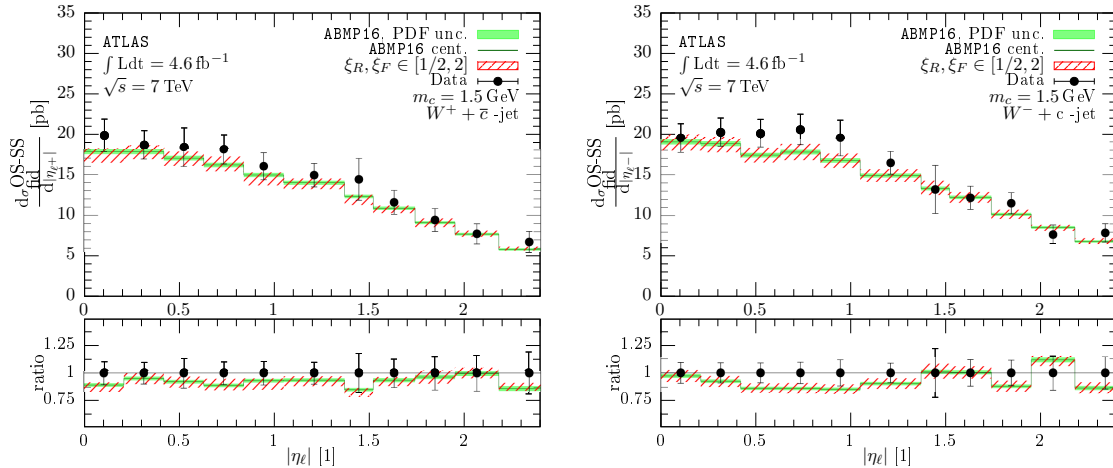


Figure 12. Same as in Fig. 9 as for the ATLAS $W + c$ -jet analysis cuts of Ref. [21].

set. Changing PYTHIA8 tune does not affect the size of scale and PDF uncertainties, as evident when comparing Fig. 10 with Fig. 9. The sizes of these bands closely resemble those obtained in the CMS analysis. For the ATLAS analysis we did not report explicitly PDF uncertainties using different PDF fits. In case of CT18NLO and CT18ZNLO PDFs, we expect that considerations analogous to those discussed for the CMS analysis apply even in the ATLAS analysis. Considering the larger uncertainty bands of these PDF fits (see Fig. 8 for the CMS case), we expect a compatibility of theory predictions and ATLAS experimental data in all bins.

For completeness we also report the comparison of our theory predictions with experimental data, in case of the c -jet analysis, published in the same ATLAS paper. Considering that, in this case, the p_T cut is bigger ($p_{T,j_c} > 25$ GeV) than for the D -meson analysis, working with hard-scattering matrix-elements, α_S and PDFs in the 3-flavour scheme, like we are doing, might not be the best solution, at least when producing fixed-order predictions, considering that logarithms of the ratio of the small charm mass with respect to large scales appearing in the partonic cross-sections might become large and then require a resummation. On the other hand, the c -jet selection criterion applied by the ATLAS collaboration, is based on the identification of at least a charmed hadron h_c inside the jet, with a low $p_{T,min}$ cut, i.e. $p_{T,h_c} > 5$ GeV. One might investigate up to which extent charm mass effects have an impact in the j_c selection process.

In practice, the level of agreement between our theory predictions at NLO+SMC accuracy and experimental data turns out to be slightly worse than the one found for the $W + D$ -meson analyses, as can be seen by comparing Fig. 12, related to $W + c$ -jet production, with Fig. 9, related to $W + D$ -meson production, with theory predictions computed with a consistent input. The uncertainty bands related to 7-point scale and ABMP16.3_NLO PDF variation in Fig. 12 have approximately the

same size as those in Fig. 9. The main difference is the fact that, while, in case of $W + D$ -meson production, central theory predictions in some bins slightly overestimate and in others slightly underestimate the experimental data, in case of $W + j_c$ production the central theory predictions systematically underestimate the central experimental datapoints by approximately $\sim (5 \div 10)\%$ and up to $\sim 15\%$ in some bins of the $|\eta_{\ell^-}|$ distribution. Theory predictions mostly lie close to the lower limit of the experimental uncertainty bands. This might point to the limitation of a three-flavour description when working with high- p_T c -jets and to the need of including higher-order corrections in the theory predictions. The level of agreement between central theory predictions and experimental data is slightly higher for forward rapidity bins, than in case of central rapidity bins. However, when considering both the experimental and theory uncertainties, one can still claim consistency between predictions and data in almost all bins. The larger disagreement is observed in the region $0.5 < |\eta_{\ell^-}| < 1$ region, which is sensitive to both d - and s -quark PDFs. In fact one can notice that the experimental differential cross-sections as a function of $|\eta_{\ell^-}|$ have a overall different shape in case of $W^+ + c$ -jet and $W^+ + D^-$ -meson production, than for the cases of $W^- + c$ -jet and $W^- + D^+$ -meson production, where the rapidity is almost constant (if not increasing) in the region $0 < \eta_{\ell^-} < 1$. These data refer to LHC Run 1. It will be interesting to cross-check our predictions with experimental results with increased statistics when they become available, especially considering that our NLO + SMC theory predictions, in contrast to data, are monotonically decreasing at increasing $|\eta_{\ell^-}|$. Unfortunately, increasing statistics will not be possible anymore at $\sqrt{s} = 7$ TeV, but a repetition of data analysis at $\sqrt{s} = 13$ TeV, with the study of additional observables, is indeed welcome and in the pipeline of the ATLAS collaboration.

As mentioned in the Introduction, a study of $W + c$ -jet production with massless charm in the 5-flavour scheme at NNLO has been recently carried out in Ref. [26]. The NNLO analysis of Ref. [26], differently from our one, led to central theory predictions which slightly overestimate most of the ATLAS central datapoints, although being still in agreement with them. The comparison with the particle-level experimental data [21] presented in Ref. [26] is however not so conclusive, being complicated (i) by the fact that it is based on fixed-order theory predictions, i.e. no parton shower + hadronization + MPI and underlying event effects were included and (ii) by the use of the flavoured- k_T jet algorithm that, although being a fully consistent choice for reconstructing a charm jet in a NNLO calculation, differs from the anti- k_T jet algorithm used in practice in the LHC experimental analyses published so far. On the other hand, in our analysis hard-scattering matrix-elements are just accurate to NLO, but parton shower, hadronization, MPI and underlying event effects are included using PYTHIA8 and we still use the anti- k_T jet algorithm that at NLO is still a viable choice even for massive jets.

Finally, we notice that including or not spin-correlation effects in the description

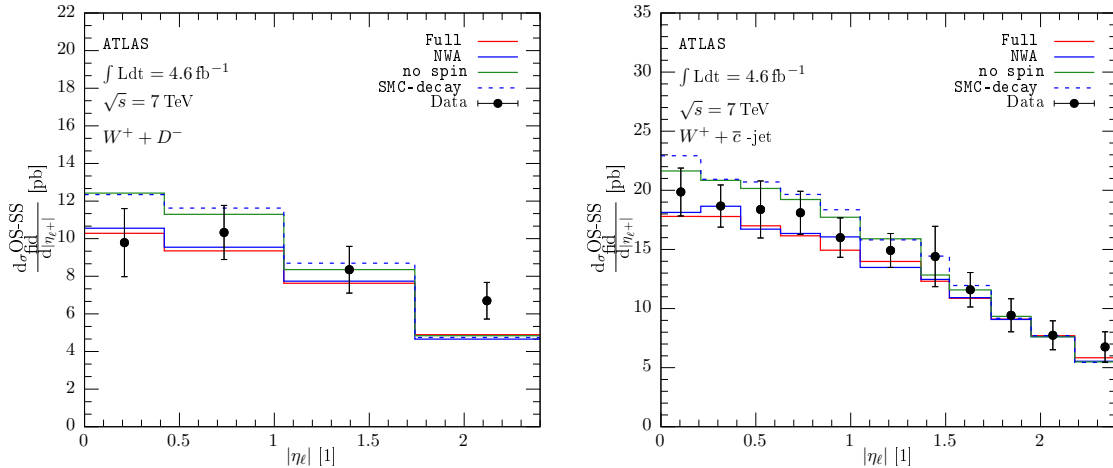


Figure 13. Left: difference of the differential cross-sections for $W + D$ -meson production, with $W^{\pm} \rightarrow \ell^{\pm} \nu_{\ell}^{(-)}$, where the ℓ^{\pm} and the hardest D^{\pm} -meson have charge of opposite sign (OS) and that where the ℓ^{\pm} and the D^{\pm} -meson have charge of the same sign (SS) as a function of the absolute value of the pseudorapidity of the hardest lepton. Theoretical predictions at NLO + SMC accuracy, obtained by PowHe1 + PYTHIA8 using different approximations, are compared to experimental data from the ATLAS collaboration [21]. In particular the results of the full simulation, including W^+ off-shell effects in PowHe1, are compared to those with W^+ decayed by PowHe1 in the NWA approximation including spin-correlation effects, to those in the NWA approximation neglecting spin-correlation effects, and to those where the W^+ boson is kept as stable in PowHe1 and decayed by PYTHIA8. The PYTHIA8 ATLAS A14 central tune with NNPDF2.3LO is used in all simulations. Right: same as in the left panel, but for the $W^+ + \bar{c}$ -jet case.

of W production and decay makes sizable changes in the shapes of the $|\eta_{\ell}|$ distributions, as can be seen in Fig. 13 and 14, which, in turn, can impact the results of PDF fits that intend to make a correct use of these data. In order to obtain reliable theory predictions for these fits, it is thus mandatory to have the most accurate possible description of W production and decay, including full off-shellness and spin-correlation effects.

4 Conclusions

We present a NLO QCD + SMC simulation of $W + c$ production, making use of the PowHe1 + PYTHIA8 approach, including charm mass effects in the hard-scattering matrix-elements, treating the W off-shell, considering spin-correlation effects and a non-diagonal CKM quark-mixing matrix. This has allowed for consistent comparisons with the already available experimental data at the particle level by the ATLAS and CMS collaborations, making use of the anti- k_T jet algorithm. Our tool/setup is

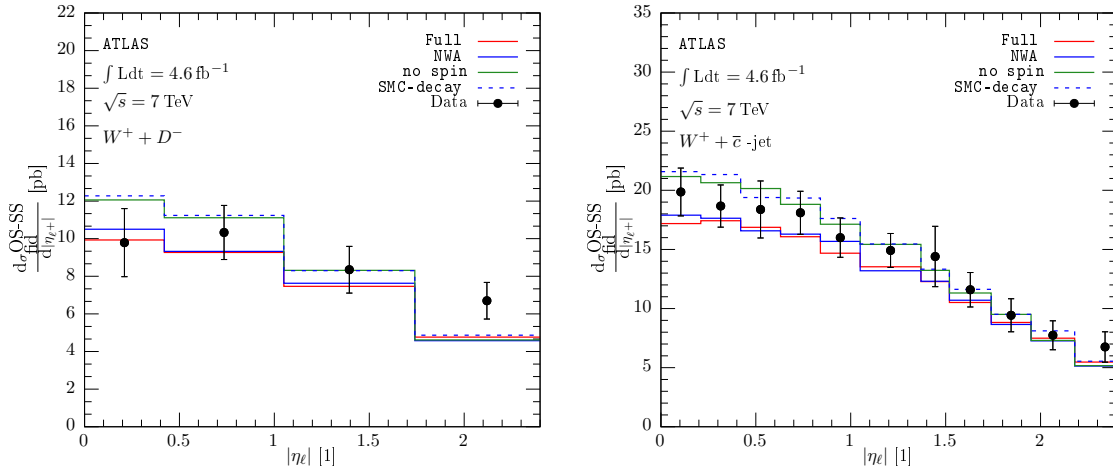


Figure 14. Same as in Fig. 13, but for the PYTHIA8 Monash tune.

particularly interesting for simulations in those experimental studies where D -mesons with relatively low p_T are reconstructed, cases in which charm mass effects can not be neglected already in the hard-scattering matrix-elements. So far, the data at the particle level obtained even in such cases have been analyzed by the experimental collaborations by making use of $W + j$ samples built using as seed hard-scattering matrix-elements with massless partons, completely neglecting charm mass effects in the hard-scattering amplitudes. Our work contributes thus to fill a gap, offering to the experimentalists a tool including charm mass and non-diagonal V_{CKM} effects for their simulations at particle level with NLO QCD + SMC accuracy. Our tool allows for comparison of the most sophisticated case, where the W boson is produced and decayed off-shell, to the simplified ones where the W boson is produced on-shell and decay in the NWA. Including or not spin-correlations in the latter case turns out to have an important effect on the shape of the distributions for which experimental data are available.

As was also noticed in Ref. [26], including or not non-diagonal V_{CKM} effects plays an important role in the simulations of $W^- + D^+$ meson and $W^- + j_c$ production, due to the fact that in these cases, not only the s -quark but even the d -quark, whose distribution function receives valence contributions differently from the s -quark one, contributes as initial state already at LO. Including non-diagonal V_{CKM} terms (in particular, a non-zero V_{cd} value) turns out to be indispensable for the correct interpretation of the data, in particular for correctly assessing the degree of strange-antistrange sea-quark asymmetry in the proton.

The agreement between our theory predictions and experimental data turns out to be similar for both ATLAS and CMS data $W + D$ -meson data, which confirms the consistency between the considered datasets and between results at different \sqrt{s} . Additionally the agreement between theory predictions and experimental data for

leptons of opposite charge is similar, which does not point to the need of extensive modifications of the strange and antistrange distribution functions in the NLO PDF fits that we used. The PDF fits adopted in this work assume that the distributions of the s and \bar{s} quarks are equal among each other, an approximation that, in the light of our results, we regard as a good one. Of course, the agreement between our theory predictions and the experimental data in case of $W^- + \bar{c}$ production would have worsened if we would have neglected the V_{cd} term, and this, in turns, would have lead to the need of assuming a larger \bar{s} distribution function with respect to the s one, in order to still reproduce the LHC experimental data. Independent measurements of V_{cd} show that the V_{cd} term is however far from being null, which support our conclusions.

Scale uncertainties amount to approximately $\pm(6 \div 8)\%$ whereas PDF uncertainties greatly vary when comparing different PDF fits, as a consequence of the different data capable of constraining quark PDFs included and of the PDF extraction methodology employed (including theoretical and parameterization input, as well as statistical aspects). We confirm the relevance of including $W + c$ data in NLO PDF fits, already pointed out by other authors. Data on the ratio of $(W^- + c)/(W^+ + \bar{c})$ have already been included by the experimental collaborations in their own QCD analyses leading to PDF fits. However, to fully exploit the constraining power of absolute cross-section data, reduced experimental uncertainties are needed.

It would be great to include these data in NNLO PDF fits. This is justified by the much smaller dependence on unphysical scales. Even greater impact could be achieved if: 1) NNLO predictions would be complemented by parton shower, hadronization and MPI effects, in order to be comparable to data at particle level in a consistent way; 2) in case a slicing method is used to regularize NNLO IR divergences, missing power corrections can hamper theoretical precision, hence the inclusion of these corrections would be fundamental; 3) charm and bottom mass effects would be included in NNLO calculations of $W + c$. Also, to make NNLO(+PS) calculations with massive quark jet(s) consistently comparable to experimental data, the jet algorithm used in the experimental analysis needs to be changed from the usual anti- k_T to a flavoured jet one, like e.g. the flavoured- k_T .

While we are confident that many of these developments will take place in the next few years, NLO calculations matched to Parton Showers as available in SMC codes can be regarded as complementary to fixed-order NNLO predictions in several respects and, for the time being, they still represent a competitive tool, although not being indeed the ultimate one, for consistent comparisons with the available experimental data on $W + c$ production. The potential of our generator and of the other available tools can be tested/challenged by forthcoming analyses, considering D -meson distributions with loose p_T cuts and observables sensitive to correlations between D mesons and leptons from W decay. New analyses in this direction are ongoing within the experimental collaborations and we look forward to future devel-

opments.

Acknowledgments

We are grateful to Lucio Cerrito, Francesco Giuli, Katerina Lipka, Sonja K. Pflitsch, for sharing with us numerous details concerning the LHC experimental analyses. We are grateful to Sergey Alekhin and Marco Guzzi for useful discussions concerning their PDF fits. We thank Sven-Olaf Moch and Pavel Nadolsky for further clarifications, and Michael Benzke and Zoltan Trocsanyi for useful suggestions.

This research was supported in part by the National Science Foundation under Grant No. NSF PHY-1748958, by grant K 125105 of the National Research, Development and Innovation Fund in Hungary, and by the Bundesministerium für Bildung und Forschung (contract 05H18GUCC1).

A Conversion to the decoupling scheme

In order to use matrix-elements in the decoupling scheme together with PDFs and α_S in different factorization/renormalization schemes, scheme conversions have to be made to get consistent predictions.

In particular we would like to make use of PDFs defined in the $\overline{\text{MS}}$ factorization scheme, with a variable number of flavours, depending on the factorization scale.

The conversion between the two schemes is process dependent and the basis for our derivation can be found in Ref. [50] for a different process. In our derivation we follow the same steps as in Ref. [50], but we adopt a slightly different notation. To fix notation we assume that the $\overline{\text{MS}}$ scheme calculation uses n_f massless quark flavours while in the decoupling scheme we have $\widetilde{n}_f = n_f - n$ massless quark flavours, where n is the number of massive quark flavours we would like to decouple. In commonly used variable flavour number PDF + α_S sets, the number of massive quarks which decouple for scales below each threshold scale is just one, i.e. massive quarks decouple one at a time, but other solutions would indeed be possible, e.g. 3 + 2 schemes. The strong couplings should coincide at the threshold scale made equal to the mass m of the lightest massive quark we would like to decouple:

$$\alpha_S^{n_f}(m) = \alpha_S^{\widetilde{n}_f}(m) + \mathcal{O}(\alpha_S^3), \quad (\text{A.1})$$

For both α_S definitions the Renormalization Group Equation (RGE) can be used to evolve them to a different scale:

$$\begin{aligned} \alpha_S^{\widetilde{n}_f}(\mu_R) &= \alpha_S^{\widetilde{n}_f}(m) - b_0^{(\widetilde{n}_f)} \alpha_S^2 \log \frac{\mu_R^2}{m^2}, \\ \alpha_S^{n_f}(\mu_R) &= \alpha_S^{\widetilde{n}_f}(m) - b_0^{(n_f)} \alpha_S^2 \log \frac{\mu_R^2}{m^2}, \end{aligned} \quad (\text{A.2})$$

with

$$b_0^{(n_f)} = \frac{11C_A - 4n_f T_R}{12\pi}. \quad (\text{A.3})$$

In the equations listed in (A.2) the scale and scheme of the strong coupling in the second terms on the right hand sides are arbitrary due to differences being introduced are of higher order. Using these formulae we can express the strong coupling in the decoupling scheme in terms of the one in the $\overline{\text{MS}}$ scheme first by exploiting Eq. (A.1), then substituting the coupling in the $\overline{\text{MS}}$ scheme at scale μ_R using the RGE:

$$\begin{aligned} \alpha_S^{(\widetilde{n}_f)}(\mu_R) &= \alpha_S^{(n_f)}(\mu_R) + \alpha_S^2 \left[b_0^{(n_f)} - b_0^{(\widetilde{n}_f)} \right] \log \frac{\mu_R^2}{m^2} = \\ &= \alpha_S^{(n_f)}(\mu_R) - \alpha_S^2 \frac{n_f T_R}{3\pi} \log \frac{\mu_R^2}{m^2}, \end{aligned} \quad (\text{A.4})$$

where in the second term on the right hand side the coupling can be evaluated in any scheme and at any scale because the introduced difference is of order $\mathcal{O}(\alpha_S^3)$, thus beyond the perturbative order we are interested in.

If the set of quarks treated as massive in the decoupling scheme is denoted as \mathcal{H} the structure function in the $\overline{\text{MS}}$ scheme fulfills

$$\begin{aligned} F_j^{(n_f)}(x, m) &= F_j^{(\widehat{n_f})}(x, m), \quad j \notin \mathcal{H}, \\ F_h^{(n_f)}(x, m_h) &= F_h^{(n_f)}(x, m_h) = 0, \quad h \in \mathcal{H}, \end{aligned} \quad (\text{A.5})$$

where m stands for the mass of the lightest heavy quark in set \mathcal{H} . To ease up notation we assume \mathcal{H} has only one member with identifier h and with mass m . To be still valid in case of multiple massive quarks in \mathcal{H} , we keep n to be general and assume that m stands for the lightest quark in set \mathcal{H} . To find the compensation terms between the $\overline{\text{MS}}$ and decoupling schemes the DGLAP equation has to be considered:

$$\frac{\partial}{\partial \log \mu^2} F_i^{(n_f)}(x, \mu) = \frac{\alpha_S^{(n_f)}(\mu)}{2\pi} \sum_j \int_x^1 \frac{dz}{z} F_j^{(n_f)}(x/z, \mu) \mathcal{P}_{ij}^{(n_f)}(z), \quad (\text{A.6})$$

where $\mathcal{P}_{ij}^{(n_f)}(z)$ is the Altarelli-Parisi (AP) kernel for $j \rightarrow i$ splitting considering n_f light quark flavours at momentum fraction z . Taking the same assumption as in Ref. [50], i.e. the mass of the lightest massive quark is of the same order of the scale, we can drop $\mathcal{O}(\alpha_S^2)$ terms and the integration of the DGLAP equation between the scale m and the scale μ is simply the integration of the coupling prefactor:

$$\begin{aligned} \int_{\log m^2}^{\log \mu^2} d \log \mu^2 \alpha_S^{(n_f)}(\mu) &= \int_{\log m^2}^{\log \mu^2} d \log \mu^2 \left[\alpha_S^{(n_f)}(m) + \alpha_S^2(\dots) \right] = \\ &= \alpha_S^{(n_f)}(m) \log \frac{\mu^2}{m^2} + \mathcal{O}(\alpha_S^2). \end{aligned} \quad (\text{A.7})$$

Using this, the integration of the DGLAP equation is trivial:

$$F_i^{(n_f)}(x, \mu) - F_i^{(n_f)}(x, m) = \frac{\alpha_S^{(n_f)}(m) \log \frac{\mu^2}{m^2}}{2\pi} \sum_j \int_x^1 \frac{dz}{z} F_j^{(n_f)}(x/z, m) \mathcal{P}_{ij}^{(n_f)}(z). \quad (\text{A.8})$$

Because the structure function for a massive quark vanishes at scales below the mass of the quark, the right hand side can be written as:

$$F_i^{(n_f)}(x, \mu) - F_i^{(n_f)}(x, m) = \frac{\alpha_S^{(n_f)}(m) \log \frac{\mu^2}{m^2}}{2\pi} \sum_{j \notin \mathcal{H}} \int_x^1 \frac{dz}{z} F_j^{(n_f)}(x/z, m) \mathcal{P}_{ij}^{(n_f)}(z). \quad (\text{A.9})$$

A similar formula can be derived in the decoupling scheme using the corresponding α_S and structure function definitions:

$$F_i^{(\widetilde{n}_f)}(x, \mu) - F_i^{(\widetilde{n}_f)}(x, m) = \frac{\alpha_S^{(\widetilde{n}_f)}(m) \log \frac{\mu^2}{m^2}}{2\pi} \sum_{j \notin \mathcal{H}} \int_x^1 \frac{dz}{z} F_j^{(\widetilde{n}_f)}(x/z, m) \mathcal{P}_{ij}^{(\widetilde{n}_f)}(z). \quad (\text{A.10})$$

In case of the integrated DGLAP equation for the $\overline{\text{MS}}$ scheme we can exploit Eq.(A.5) and Eq.(A.1) to write:

$$F_i^{(n_f)}(x, \mu) - F_i^{(\widetilde{n}_f)}(x, m) = \frac{\alpha_S^{(\widetilde{n}_f)}(m) \log \frac{\mu^2}{m^2}}{2\pi} \sum_{j \notin \mathcal{H}} \int_x^1 \frac{dz}{z} F_j^{(\widetilde{n}_f)}(x/z, m) \mathcal{P}_{ij}^{(n_f)}(z). \quad (\text{A.11})$$

Hence the difference between Eq.(A.11) and Eq.(A.16) takes the form of:

$$\begin{aligned} F_i^{(n_f)}(x, \mu) - F_i^{(\widetilde{n}_f)}(x, \mu) &= \\ &= \frac{\alpha_S^{(\widetilde{n}_f)}(m) \log \frac{\mu^2}{m^2}}{2\pi} \sum_{j \notin \mathcal{H}} \int_x^1 \frac{dz}{z} F_j^{(\widetilde{n}_f)}(x/z, m) \left[\mathcal{P}_{ij}^{(n_f)}(z) - \mathcal{P}_{ij}^{(\widetilde{n}_f)}(z) \right]. \end{aligned} \quad (\text{A.12})$$

Taking a look at the AP kernels, like Eq.(2.33) in Ref.[64], reveals that only the $g \rightarrow g$ splitting kernel depends on the number of light quark flavours such that the difference is

$$\mathcal{P}_{gg}^{(n_f)}(z) - \mathcal{P}_{gg}^{(\widetilde{n}_f)}(z) = -\frac{2n}{3} T_R \delta(1-z). \quad (\text{A.13})$$

Thus, we can conclude that

$$\begin{aligned} F_j^{(n_f)}(x, \mu) - F_j^{(\widetilde{n}_f)}(x, \mu) &= 0, \quad j \neq g, j \notin \mathcal{H}, \\ F_g^{(n_f)}(x, \mu) - F_g^{(\widetilde{n}_f)}(x, \mu) &= -\frac{2n}{3} T_R \frac{\alpha_S^{(\widetilde{n}_f)}(m) \log \frac{\mu^2}{m^2}}{2\pi} F_g^{(\widetilde{n}_f)}(x, m). \end{aligned} \quad (\text{A.14})$$

Using

$$\alpha_S F_g^{(\widetilde{n}_f)}(x, m) = \alpha_S F_g^{(\widetilde{n}_f)}(x, \mu) + \mathcal{O}(\alpha_S^2), \quad (\text{A.15})$$

we find

$$\begin{aligned} F_j^{(n_f)}(x, \mu) &= F_j^{(\widetilde{n}_f)}(x, \mu) + \mathcal{O}(\alpha_S^2), \quad j \neq g, j \notin \mathcal{H}, \\ F_g^{(n_f)}(x, \mu) &= F_g^{(\widetilde{n}_f)}(x, \mu) \left(1 - \alpha_S^{(\widetilde{n}_f)}(m) \frac{n T_R}{3\pi} \log \frac{\mu^2}{m^2} \right) + \mathcal{O}(\alpha_S^2). \end{aligned} \quad (\text{A.16})$$

In case of $W + c$ production the Born level partonic processes can only have initial states $\overset{(-)}{q}g$ and $g\overset{(-)}{q}$. Due to symmetry and to ease notation we only consider the qg channel. The integrand of the convolution integral of the Collinear Factorization Theorem reads in the $\overline{\text{MS}}$ scheme

$$F_q^{(n_f)}(x_1, \mu_F) F_g^{(n_f)}(x_1, \mu_F) \sigma_{qg}^{(0)} = F_q^{(n_f)}(x_1, \mu_F) F_g^{(n_f)}(x_1, \mu_F) \alpha_S^{(n_f)}(\mu_R) f_{qg}^{(0)}, \quad (\text{A.17})$$

where $f_{qg}^{(0)}$ is the $\overline{\text{MS}}$ partonic cross section for the initial state qg with strong coupling factorized out. To turn the Factorization Theorem from the $\overline{\text{MS}}$ scheme to a form valid in the decoupling scheme, Eqs.(A.4) and (A.16) can be used:

$$\begin{aligned} F_q^{(n_f)}(x_1, \mu_F) F_g^{(n_f)}(x_1, \mu_F) \alpha_S^{(n_f)}(\mu_R) f_{qg}^{(0)} &= F_q^{(\widetilde{n}_f)}(x_1, \mu_F) F_g^{(\widetilde{n}_f)}(x_1, \mu_F) \alpha_S^{(\widetilde{n}_f)}(\mu_R) f_{qg}^{(0)} \\ &\cdot \left(1 - \alpha_S^{(\widetilde{n}_f)}(m) \frac{n T_R}{3\pi} \log \frac{\mu_F^2}{m^2} \right) \cdot \left(1 + \alpha_S^{(\widetilde{n}_f)}(m) \frac{n T_R}{3\pi} \log \frac{\mu_R^2}{m^2} \right) = \\ &= \left(1 + \alpha_S^{(\widetilde{n}_f)}(m) \frac{n T_R}{3\pi} \log \frac{\mu_R^2}{\mu_F^2} \right) F_q^{(\widetilde{n}_f)}(x_1, \mu_F) F_g^{(\widetilde{n}_f)}(x_1, \mu_F) \alpha_S^{(\widetilde{n}_f)}(\mu_R) f_{qg}^{(0)}. \end{aligned} \quad (\text{A.18})$$

This expression allows us to use PDFs and α_S with \widetilde{n}_f light quark flavours in the decoupling scheme together with a partonic cross-section in the $\overline{\text{MS}}$ scheme. Or, by multiplying with the inverse of the prefactor and expanding it perturbatively, it allows for using a PDF and corresponding α_S defined in the $\overline{\text{MS}}$ scheme in a calculational framework defined in the decoupling scheme.

Note that as long as the non-physical scales coincide the compensation term is identically zero, so it is only needed for scale variations if $\mu_R = \mu_F$ and in general when different choices are made for the factorization and renormalization scales. Note also that the compensation term is of order $\mathcal{O}(\alpha_S^2)$ hence it is the same order as the NLO correction to the partonic cross-section. Because of this, the compensation only affects the Born contribution in the NLO calculation, where terms of order $\mathcal{O}(\alpha_S^3)$ are dropped.

References

- [1] A. Accardi *et. al.*, *A Critical Appraisal and Evaluation of Modern PDFs*, *Eur. Phys. J.* **C76** (2016), no. 8 471, [[arXiv:1603.08906](#)].
- [2] **PROSA** Collaboration, O. Zenaiev *et. al.*, *Impact of heavy-flavour production cross sections measured by the LHCb experiment on parton distribution functions at low x* , *Eur. Phys. J.* **C75** (2015), no. 8 396, [[arXiv:1503.04581](#)].
- [3] V. Bertone, R. Gauld, and J. Rojo, *Neutrino Telescopes as QCD Microscopes*, *JHEP* **01** (2019) 217, [[arXiv:1808.02034](#)].
- [4] **PROSA** Collaboration, O. Zenaiev, M. V. Garzelli, K. Lipka, S. O. Moch, A. Cooper-Sarkar, F. Olness, A. Geiser, and G. Sigl, *Improved constraints on parton distributions using LHCb, ALICE and HERA heavy-flavour measurements and implications for the predictions for prompt atmospheric-neutrino fluxes*, *JHEP* **04** (2020) 118, [[arXiv:1911.13164](#)].
- [5] S. Alekhin, J. Blumlein, L. Caminadac, K. Lipka, K. Lohwasser, S. Moch, R. Petti, and R. Placakyte, *Determination of Strange Sea Quark Distributions from Fixed-target and Collider Data*, *Phys. Rev.* **D91** (2015), no. 9 094002, [[arXiv:1404.6469](#)].
- [6] S. Alekhin, J. Blumlein, and S. Moch, *Strange sea determination from collider data*, *Phys. Lett.* **B777** (2018) 134–140, [[arXiv:1708.01067](#)].
- [7] F. Faura, S. Iranipour, E. R. Nocera, J. Rojo, and M. Ubiali, *The Strangest Proton?*, *Eur. Phys. J.* **C80** (2020), no. 12 1168, [[arXiv:2009.00014](#)].
- [8] **xFitter Developers’ Team** Collaboration, H. Abdolmaleki *et. al.*, *Probing the strange content of the proton with charm production in charged current at LHeC*, *Eur. Phys. J.* **C79** (2019), no. 10 864, [[arXiv:1907.01014](#)].
- [9] M. Garzelli, “QCD opportunities at a Forthcoming Forward Physics Facility.” Poster presentation at the APS 2021 April Meeting, 2021.
- [10] **CMS** Collaboration, A. M. Sirunyan *et. al.*, *A search for the standard model Higgs boson decaying to charm quarks*, *JHEP* **03** (2020) 131, [[arXiv:1912.01662](#)].
- [11] **ATLAS** Collaboration, T. A. collaboration, *Direct constraint on the Higgs-charm coupling from a search for Higgs boson decays to charm quarks with the ATLAS detector*, .
- [12] S. Iwamoto, G. Lee, Y. Shadmi, and Y. Weiss, *Tagging new physics with charm*, *JHEP* **09** (2017) 114, [[arXiv:1703.05748](#)].
- [13] **ATLAS** Collaboration, M. Aaboud *et. al.*, *Search for dark matter and other new phenomena in events with an energetic jet and large missing transverse momentum using the ATLAS detector*, *JHEP* **01** (2018) 126, [[arXiv:1711.03301](#)].
- [14] **CMS** Collaboration, A. M. Sirunyan *et. al.*, *Search for dark matter produced in*

- association with heavy-flavor quark pairs in proton-proton collisions at $\sqrt{s} = 13$ TeV, *Eur. Phys. J. C* **77** (2017), no. 12 845, [[arXiv:1706.02581](#)].
- [15] G. C. Branco, P. M. Ferreira, L. Lavoura, M. N. Rebelo, M. Sher, and J. P. Silva, *Theory and phenomenology of two-Higgs-doublet models*, *Phys. Rept.* **516** (2012) 1–102, [[arXiv:1106.0034](#)].
- [16] **CDF** Collaboration, T. Aaltonen *et. al.*, *First measurement of the production of a W boson in association with a single charm quark in $p\bar{p}$ collisions at $\sqrt{s} = 1.96$ -TeV*, *Phys. Rev. Lett.* **100** (2008) 091803, [[arXiv:0711.2901](#)].
- [17] **D0** Collaboration, V. M. Abazov *et. al.*, *Measurement of the ratio of the $p\bar{p} \rightarrow W^+c^-$ jet cross section to the inclusive $p\bar{p} \rightarrow W + \text{jets}$ cross section*, *Phys. Lett. B* **666** (2008) 23–30, [[arXiv:0803.2259](#)].
- [18] **CDF** Collaboration, T. Aaltonen *et. al.*, *Observation of the Production of a W Boson in Association with a Single Charm Quark*, *Phys. Rev. Lett.* **110** (2013), no. 7 071801, [[arXiv:1209.1921](#)].
- [19] **CMS** Collaboration, C. Collaboration, *Measurement of the associated production of a W boson and a charm quark at $\sqrt{s} = 8$ TeV*, .
- [20] **CMS** Collaboration, S. Chatrchyan *et. al.*, *Measurement of Associated $W + \text{Charm}$ Production in pp Collisions at $\sqrt{s} = 7$ TeV*, *JHEP* **02** (2014) 013, [[arXiv:1310.1138](#)].
- [21] **ATLAS** Collaboration, G. Aad *et. al.*, *Measurement of the production of a W boson in association with a charm quark in pp collisions at $\sqrt{s} = 7$ TeV with the ATLAS detector*, *JHEP* **05** (2014) 068, [[arXiv:1402.6263](#)].
- [22] **CMS** Collaboration, A. M. Sirunyan *et. al.*, *Measurement of associated production of a W boson and a charm quark in proton-proton collisions at $\sqrt{s} = 13$ TeV*, *Eur. Phys. J. C* **79** (2019), no. 3 269, [[arXiv:1811.10021](#)].
- [23] **LHCb** Collaboration, R. Aaij *et. al.*, *Study of W boson production in association with beauty and charm*, *Phys. Rev. D* **92** (2015), no. 5 052001, [[arXiv:1505.04051](#)].
- [24] J. M. Campbell, R. K. Ellis, and W. T. Giele, *A Multi-Threaded Version of MCFM*, *Eur. Phys. J. C* **75** (2015), no. 6 246, [[arXiv:1503.06182](#)].
- [25] W. J. Stirling and E. Vryonidou, *Charm production in association with an electroweak gauge boson at the LHC*, *Phys. Rev. Lett.* **109** (2012) 082002, [[arXiv:1203.6781](#)].
- [26] M. Czakon, A. Mitov, M. Pellen, and R. Poncelet, *NNLO QCD predictions for $W+c$ -jet production at the LHC*, [[arXiv:2011.01011](#)].
- [27] J. Alwall, R. Frederix, S. Frixione, V. Hirschi, F. Maltoni, O. Mattelaer, H. S. Shao, T. Stelzer, P. Torrielli, and M. Zaro, *The automated computation of tree-level and next-to-leading order differential cross sections, and their matching to parton shower simulations*, *JHEP* **07** (2014) 079, [[arXiv:1405.0301](#)].

- [28] P. Nason, *A New method for combining NLO QCD with shower Monte Carlo algorithms*, *JHEP* **11** (2004) 040, [[hep-ph/0409146](#)].
- [29] S. Frixione, P. Nason, and C. Oleari, *Matching NLO QCD computations with Parton Shower simulations: the POWHEG method*, *JHEP* **11** (2007) 070, [[arXiv:0709.2092](#)].
- [30] J. C. Collins, F. Wilczek, and A. Zee, *Low-Energy Manifestations of Heavy Particles: Application to the Neutral Current*, *Phys. Rev.* **D18** (1978) 242.
- [31] M. Cacciari, G. P. Salam, and G. Soyez, *The anti- k_t jet clustering algorithm*, *JHEP* **04** (2008) 063, [[arXiv:0802.1189](#)].
- [32] A. Banfi, G. P. Salam, and G. Zanderighi, *Infrared safe definition of jet flavor*, *Eur. Phys. J.* **C47** (2006) 113–124, [[hep-ph/0601139](#)].
- [33] J. Rojo, *Progress in the NNPDF global analyses of proton structure*, in *55th Rencontres de Moriond on QCD and High Energy Interactions*, 4, 2021. [[arXiv:2104.09174](#)].
- [34] NNPDF Collaboration, R. D. Ball *et. al.*, *Parton distributions from high-precision collider data*, *Eur. Phys. J.* **C77** (2017), no. 10 663, [[arXiv:1706.00428](#)].
- [35] S. Bailey, T. Cridge, L. A. Harland-Lang, A. D. Martin, and R. S. Thorne, *Parton distributions from LHC, HERA, Tevatron and fixed target data: MSHT20 PDFs*, *Eur. Phys. J.* **C81** (2021), no. 4 341, [[arXiv:2012.04684](#)].
- [36] T.-J. Hou *et. al.*, *New CTEQ global analysis of quantum chromodynamics with high-precision data from the LHC*, *Phys. Rev.* **D103** (2021), no. 1 014013, [[arXiv:1912.10053](#)].
- [37] S. Alioli, P. Nason, C. Oleari, and E. Re, *A general framework for implementing NLO calculations in shower Monte Carlo programs: the POWHEG BOX*, *JHEP* **06** (2010) 043, [[arXiv:1002.2581](#)].
- [38] G. Bevilacqua, M. Czakon, M. V. Garzelli, A. van Hameren, A. Kardos, C. G. Papadopoulos, R. Pittau, and M. Worek, *HELAC-NLO*, *Comput. Phys. Commun.* **184** (2013) 986–997, [[arXiv:1110.1499](#)].
- [39] S. Frixione, Z. Kunszt, and A. Signer, *Three jet cross-sections to next-to-leading order*, *Nucl. Phys. B* **467** (1996) 399–442, [[hep-ph/9512328](#)].
- [40] S. Frixione, *A General approach to jet cross-sections in QCD*, *Nucl. Phys. B* **507** (1997) 295–314, [[hep-ph/9706545](#)].
- [41] T. Sjöstrand, *The PYTHIA Event Generator: Past, Present and Future*, *Comput. Phys. Commun.* **246** (2020) 106910, [[arXiv:1907.09874](#)].
- [42] T. Sjöstrand, S. Ask, J. R. Christiansen, R. Corke, N. Desai, P. Ilten, S. Mrenna, S. Prestel, C. O. Rasmussen, and P. Z. Skands, *An introduction to pythia 8.2*, *Computer Physics Communications* **191** (Jun, 2015) 159–177.

- [43] T. Sjostrand, S. Mrenna, and P. Z. Skands, *PYTHIA 6.4 Physics and Manual*, *JHEP* **05** (2006) 026, [[hep-ph/0603175](#)].
- [44] J. Bellm *et. al.*, *Herwig 7.2 release note*, *Eur. Phys. J. C* **80** (2020), no. 5 452, [[arXiv:1912.06509](#)].
- [45] G. Corcella, I. G. Knowles, G. Marchesini, S. Moretti, K. Odagiri, P. Richardson, M. H. Seymour, and B. R. Webber, *HERWIG 6: An Event generator for hadron emission reactions with interfering gluons (including supersymmetric processes)*, *JHEP* **01** (2001) 010, [[hep-ph/0011363](#)].
- [46] G. Corcella, I. G. Knowles, G. Marchesini, S. Moretti, K. Odagiri, P. Richardson, M. H. Seymour, and B. R. Webber, *HERWIG 6.5 release note*, [hep-ph/0210213](#).
- [47] G. Bevilacqua, M. V. Garzelli, and A. Kardos, *$t\bar{t}b\bar{b}$ hadroproduction with massive bottom quarks with PowHel*, [arXiv:1709.06915](#).
- [48] M. V. Garzelli, A. Kardos, and Z. Trócsányi, *Hadroproduction of $t\bar{t}b\bar{b}$ final states at LHC: predictions at NLO accuracy matched with Parton Shower*, *JHEP* **03** (2015) 083, [[arXiv:1408.0266](#)].
- [49] A. Buckley, J. Ferrando, S. Lloyd, K. Nordstrom, B. Page, M. Rofenacht, M. Schonherr, and G. Watt, *LHAPDF6: parton density access in the LHC precision era*, *Eur. Phys. J. C* **75** (2015) 132, [[arXiv:1412.7420](#)].
- [50] M. Cacciari, M. Greco, and P. Nason, *The $P(T)$ spectrum in heavy flavor hadroproduction*, *JHEP* **05** (1998) 007, [[hep-ph/9803400](#)].
- [51] J. Campbell and T. Neumann, *Precision Phenomenology with MCFM*, *JHEP* **12** (2019) 034, [[arXiv:1909.09117](#)].
- [52] S. Alekhin, J. Blümlein, and S. Moch, *NLO PDFs from the ABMP16 fit*, *Eur. Phys. J. C* **78** (2018), no. 6 477, [[arXiv:1803.07537](#)].
- [53] T.-J. Hou *et. al.*, *Progress in the CTEQ-TEA NNLO global QCD analysis*, [arXiv:1908.11394](#).
- [54] C. Collaboration. Private communication, 2021.
- [55] S. Alioli, P. Nason, C. Oleari, and E. Re, *NLO Higgs boson production via gluon fusion matched with shower in POWHEG*, *JHEP* **04** (2009) 002, [[arXiv:0812.0578](#)].
- [56] S. Alioli, P. Nason, C. Oleari, and E. Re, *NLO vector-boson production matched with shower in POWHEG*, *JHEP* **07** (2008) 060, [[arXiv:0805.4802](#)].
- [57] P. Skands, S. Carrazza, and J. Rojo, *Tuning PYTHIA 8.1: the Monash 2013 Tune*, *Eur. Phys. J. C* **74** (2014), no. 8 3024, [[arXiv:1404.5630](#)].
- [58] **ATLAS** Collaboration, *ATLAS Pythia 8 tunes to 7 TeV data*, .
- [59] R. D. Ball *et. al.*, *Parton distributions with LHC data*, *Nucl. Phys. B* **867** (2013) 244–289, [[arXiv:1207.1303](#)].
- [60] P. Marquard, A. V. Smirnov, V. A. Smirnov, and M. Steinhauser, *Quark mass*

relations to four-loop order in perturbative qcd, *Physical Review Letters* **114** (Apr, 2015).

- [61] M. V. Garzelli, L. Kemmler, S. Moch, and O. Zenaiev, *Heavy-flavor hadro-production with heavy-quark masses renormalized in the $\overline{\text{MS}}$, MSR and on-shell schemes*, *JHEP* **04** (2021) 043, [[arXiv:2009.07763](#)].
- [62] S. Alekhin, A. Kardos, S. Moch, and Z. Trocsanyi, *Precision studies for Drell-Yan processes at NNLO*, [arXiv:2104.02400](#).
- [63] M. A. Ebert, J. K. L. Michel, I. W. Stewart, and F. J. Tackmann, *Drell-Yan $q\bar{q}$ resummation of fiducial power corrections at N^3LL* , *JHEP* **04** (2021) 102, [[arXiv:2006.11382](#)].
- [64] J. Campbell, J. Huston, and F. Krauss, *The Black Book of Quantum Chromodynamics: A Primer for the LHC Era*. Oxford University Press, 12, 2017.